Acta Neuropathologica (2019) 138:913–941
https://doi.org/10.1007/s00401-019-02053-5

ORIGINAL PAPER

Aβ-induced acceleration of Alzheimer-related τ-pathology spreading and its association with prion protein

Luis Aragão Gomes[1,2] · Silvia Andrea Hipp[3,4] · Ajeet Rijal Upadhaya[3] · Karthikeyan Balakrishnan[3,5] · Simona Ospitalieri[1,2] · Marta J. Koper[1,2,6,7] · Pablo Largo-Barrientos[7,8] · Valerie Uytterhoeven[7,8] · Julia Reichwald[9] · Sabine Rabe[9] · Rik Vandenberghe[2,10,11] · Christine A. F. von Arnim[12,13] · Thomas Tousseyn[14] · Regina Feederle[15,16,17] · Camilla Giudici[16] · Michael Willem[18] · Matthias Staufenbiel[9] · Dietmar Rudolf Thal[1,2,3,14]

Received: 8 January 2019 / Revised: 26 July 2019 / Accepted: 31 July 2019 / Published online: 14 August 2019

Abstract

Extracellular deposition of amyloid β-protein (Aβ) in amyloid plaques and intracellular accumulation of abnormally phosphorylated τ-protein (p-τ) in neurofibrillary tangles (NFTs) represent pathological hallmark lesions of Alzheimer's disease (AD). Both lesions develop in parallel in the human brain throughout the preclinical and clinical course of AD. Nevertheless, it is not yet clear whether there is a direct link between Aβ and τ pathology or whether other proteins are involved in this process. To address this question, we crossed amyloid precursor protein (APP) transgenic mice overexpressing human APP with the Swedish mutation (670/671 KM → NL) (APP23), human wild-type APP (APP51/16), or a proenkephalin signal peptide linked to human $Aβ_{42}$ (APP48) with τ-transgenic mice overexpressing human mutant 4-repeat τ-protein with the P301S mutation (TAU58). In 6-month-old APP23xTAU58 and APP51/16xTAU58 mice, soluble Aβ was associated with the aggravation of p-τ pathology propagation into the CA1/subiculum region, whereas 6-month-old TAU58 and APP48xTAU58 mice neither exhibited significant amounts of p-τ pathology in the CA1/subiculum region nor displayed significant levels of soluble Aβ in the forebrain. In APP23xTAU58 and APP51/16xTAU58 mice showing an acceleration of p-τ propagation, Aβ and p-τ were co-immunoprecipitated with cellular prion protein (PrP^C). A similar interaction between PrP^C, p-τ and Aβ was observed in human AD brains. This association was particularly noticed in 60% of the symptomatic AD cases in our sample, suggesting that PrP^C may play a role in the progression of AD pathology. An in vitro pull-down assay confirmed that PrP^C is capable of interacting with Aβ and p-τ. Using a proximity ligation assay, we could demonstrate proximity (less than ~ 30–40 nm distance) between PrP^C and Aβ and between PrP^C and p-τ in APP23xTAU58 mouse brain as well as in human AD brain. Proximity between PrP^C and p-τ was also seen in APP51/16xTAU58, APP48xTAU58, and TAU58 mice. Based on these findings, it is tempting to speculate that PrP^C is a critical player in the interplay between Aβ and p-τ propagation at least in a large group of AD cases. Preexisting p-τ pathology interacting with PrP^C, thereby, appears to be a prerequisite for Aβ to function as a p-τ pathology accelerator via PrP^C.

Keywords Tau-protein · Amyloid-β · Cross seeding · Alzheimer's disease · Transgenic mice · Neuropathology · Prion protein

Introduction

Alzheimer's disease is histopathologically characterized by the extracellular deposition of amyloid β-protein (Aβ) in senile plaques [58] and by intraneuronal neurofibrillary tangles (NFTs) consisting of aggregated abnormal phosphorylated τ protein (p-τ) [33, 34]. Both, Aβ and p-τ-pathology spread throughout the brain in a hierarchical pattern. However, Aβ plaques initially appear in the cerebral neocortex, whereas NFTs start to develop in the transentorhinal

Luis Aragão Gomes and Silvia Andrea Hipp have contributed equally and are listed in alphabetical order.

Electronic supplementary material The online version of this article (https://doi.org/10.1007/s00401-019-02053-5) contains supplementary material, which is available to authorized users.

✉ Dietmar Rudolf Thal
Dietmar.Thal@kuleuven.be

Extended author information available on the last page of the article

region of the allocortex [9, 91]. Prior to NFT formation in the transentorhinal region, accumulation of p-τ has been observed in the locus coeruleus, the raphe nuclei, substantia nigra, dorsal nucleus of the vagal nerve, and the basal nucleus of Meynert [4, 11, 12, 32]. Although both pathologies follow different neuroanatomical routes of propagation [10, 91], after a certain stage, Aβ plaques and NFTs are both found in neocortical brain regions [2, 9, 91]. The expansion of neurodegenerative lesions from one brain region to another is often referred to as "spreading" or "propagation", and can be influenced by neurogenetic factors [81]. Here, we use the terms "spreading" and "propagation" as explained.

In transgenic mouse models, it was demonstrated that injection of Aβ into the brains of τ-transgenic mice exacerbates τ-pathology and that crossbreeding of τ and amyloid precursor protein (APP) overexpressing transgenic mice also leads to enhanced p-τ-pathology, in comparison with single τ-transgenic mice [30, 54]. Prevalent Aβ plaque pathology increased the seeding effect of AD-paired helical filament τ-aggregates [99] and lead to the development not only of NFTs but also of neuritic plaques, i.e., a subset of Aβ plaques that exhibits dystrophic neurites with p-τ pathology [38]. Furthermore, treatment of a triple transgenic mouse model overexpressing mutant APP (670/671 KM → NL), mutant presenilin 1 (M146V), and mutant τ (P301L) with anti-Aβ antibodies leads to a decrease of Aβ plaques and NFTs in the treated animals [65]. Nevertheless, it is not yet clear how Aβ and τ pathology interact and whether other proteins are involved in this process.

Recently, cellular prion protein (PrP^C) was reported as a receptor for toxic Aβ species as well as for α-synuclein oligomers [25, 53]. PrP^C was required for both Aβ and α-synuclein-mediated synaptic dysfunction and memory deficits in transgenic mouse models [25, 29, 53]. In the human brain, PrP^C occurs in the neuropil of the gray matter and in neurons [23, 72]. PrP^C in AD cases had been detected in amyloid plaques and neurons [23, 26, 86, 98]. Within amyloid plaques, also dystrophic neurites of neuritic plaques exhibited PrP^C [86]. The total levels of PrP^C in AD cases were lower than in non-AD control cases, which were related to a reduced number of PrP^C-expressing neurons in AD cortex [98, 106, 107]. Furthermore, a study in iPSC-derived neurons suggested that τ effects on synaptic disruption are blocked by PrP^C inhibition [42]. PrP^C was also considered to be enriched in postsynaptic densities leading to Fyn kinase activation, which in turn phosphorylates the GluN2B subunit of NMDA receptors [94]. In addition, Fyn phosphorylation of τ has been widely demonstrated [47, 52, 62, 64]. Since Aβ oligomers can initiate PrP^C–Fyn-related phosphorylation of τ [51], the question arises whether PrP^C is involved in the interplay between Aβ and p-τ pathology propagation.

Here, we used transgenic mouse models to clarify the interaction between Aβ and p-τ pathology, the involvement of PrP^C in this mechanism, and its relevance for the spreading of p-τ pathology. We found that mice overexpressing higher levels of soluble, presumably extracellular, APP-derived Aβ, showed accelerated p-τ spreading accompanied by binding of Aβ and p-τ to PrP^C in co-immunoprecipitation and proximity ligation assays. Such an association was also observed in human AD brain samples.

Materials and methods

Animals

Generation of APP23 mice was performed as previously described [85] and continuously back-crossed to C57BL/6. To drive neuron-specific overexpression of human APP751 harboring the Swedish double mutation 670/671 KM → NL in APP23 mice, a murine Thy-1 cassette was used as promoter. Likewise, APP51/16 mice were generated as described previously [39, 73] and continuously back-crossed to C57BL/6. Here, a murine Thy-1 promoter was used to drive neuron-specific expression of human wild-type APP in a similar extent as the transgene was expressed in APP23 mice. Generation of APP48 mice was performed as previously described [1]. These mice were continuously back-crossed to C57BL/6. In APP48 mice, a murine Thy-1 expression cassette was used to drive neuron-specific expression of the rat proenkephalin signal sequence followed by human wild-type $Aβ_{1–42}$ to drive neuron-specific expression of human wild-type $Aβ_{1–42}$. Thereby, $Aβ_{1–42}$ is released into the endoplasmic reticulum and the Golgi apparatus independent from APP metabolism [1]. Finally, TAU58 mice were generated as described previously [95]. These mice overexpress mutant (P301S) τ-protein for the 363 amino acid isoform of human four-repeat τ-protein driven by a Thy-1 promoter and develop accumulations of p-τ in brainstem and few neocortical neurons at the age of 3 months [95].

TAU58 mice were crossbred with (1) APP23 mice, (2) APP51/16 mice, and (3) APP48 mice. Genotyping was performed by PCR from mouse ear tissue (ear patches) [1, 85]. APP23xTAU58, APP51/16xTAU58, and APP48x-TAU58 mice heterozygous for both transgenes were euthanized by decapitation at 6 months of age after isoflurane anesthesia.

Six-month-old TAU58 mice and APP-transgenic mice served as single transgenic controls.

All crossbreeding experiments and mouse euthanasia were performed at the Novartis Institutes for Biomedical Research in Basel with permission in agreement with the

Swiss law for the use of laboratory animals (permissions nos. BS-1795, BW-1094, and BW-444).

Human autopsy cases

Human brains from 19 autopsy cases of both sexes (10 AD, 5 p-preAD (pathologically defined preclinical AD [74], and 4 non-AD controls) were investigated (Table 1). The brains were collected at university hospitals in Germany (Bonn and Ulm) and Belgium (Leuven). Autopsies were performed in accordance with German/Belgian law and were used for this study after receiving a positive vote from the local ethical committees in Ulm/Germany (no. 86/13) and Leuven/Belgium (no. S-59295).

The non-AD and p-preAD patients were examined at the time point of hospital admission (approximately 1–4 weeks prior to death) by clinicians with different specialties according to standardized protocols. The AD patients were diagnosed by a neurologist (RV, CAFvA) and followed until death. The protocols included the assessment of cognitive function (orientation to place, time and person; specific cognitive or neuropsychiatric tests were not performed) and recorded the patients' ability to care for themselves and to get dressed, eating habits, bladder and bowel continence, speech patterns, writing and reading ability, short-term and long-term memory, and orientation within the hospital setting. These data were used to retrospectively assess the clinical dementia rating (CDR) scores for each patient [43] without knowledge of the pathological diagnosis. For this purpose, the information from the clinical files was used to provide a CDR score according to the standard CDR protocol [43].

Neuropathology

Mouse samples

One hemisphere of the mouse brains was embedded in paraffin, whereas the second hemisphere was kept snap frozen at − 80 °C. Paraffin sections were cut at 4 µm. The Gallyas silver staining technique [8] was used for diagnosis and detection of NFTs.

Human samples

The left brain hemispheres were fixed in a 4% aqueous or phosphate-buffered solution of formaldehyde for approx. 2–4 weeks. After dissection of the brainstem and cerebellum from the forebrain, the forebrain was cut into 1 cm frontal slabs. Brain stem and cerebellum were cut perpendicular to the Meynert brain stem axis in 0.5 cm slabs. For histological assessments, tissue blocks from frontal, parietal, and occipital lobe (Area 17), cingulate gyrus, hippocampus with temporal cortex, entorhinal cortex, hypothalamus, basal ganglia, amygdala, basal nucleus of Meynert, thalamus, midbrain, pons, medulla oblongata, and cerebellum were dissected, embedded in paraffin, and microtomed at 5–12 µm. For neuropathological diagnosis, paraffin sections were stained with hematoxylin and eosin (H&E). None of the cases included in this study showed signs of hypoxemia-related neuron damage. The right brain hemispheres were sliced into 1 cm-thick frontal slabs and large parts, including the medial temporal lobe, were kept frozen at − 80 °C, whereas residual material was kept fixed in 4% aqueous or phosphate-buffered solution of formaldehyde.

Immunohistochemistry

Paraffin-embedded tissue sections from 6-month-old APP23xTAU58 ($n = 13$), APP51/16xTAU58 ($n = 8$), APP48xTAU58 ($n = 11$), and TAU58 mice ($n = 18$) as well as from medial temporal lobe and occipital cortex of human cases nos. 1–6 and 8–19 were used for immunohistochemical analysis. From case no. 7, only frozen tissue and the neuropathological diagnosis were available. Immunohistochemistry was performed with antibodies against p-τ (AT8, 1/1000, microwave pretreatment, Pierce-Thermo Scientific, MA, USA; PHF-1, 1/250, microwave pretreatment, gift of Dr. P. Davies, New York [69]; TG-3, 1/10, monoclonal IgM antibody, gift of Dr. P. Davies, New York [48]), 3-repeat τ (RD3, 1/500, microwave and formic acid pretreatment, Millipore, Burlington, MA, USA), 4-repeat τ (RD4, 1000, microwave and formic acid pretreatment, Millipore, Burlington, MA, USA), $A\beta_{17–24}$ (4G8, 1/1000, formic acid pretreatment, Covance, Dedham, MA, USA), $A\beta_{1–17}$ (6E10, 1/1000, formic acid pretreatment, Covance, Dedham, MA, USA), $A\beta_{42}$ (polyclonal rabbit, 1/100, formic acid pretreatment, IBL, Minneapolis, MN, USA), $A\beta_{40}$ (polyclonal rabbit,1/100, formic acid pretreatment, IBL, Minneapolis, MN, USA), and PrP^{C} (3F4, 1/100, formic acid and heat pretreatment, Millipore, Burlington, MA, USA; 6D11, 1/250, formic acid and heat pretreatment, Biologend, San Diego, CA, USA). The rat monoclonal $A\beta_{42/43}$ specific antibody 13D6 (IgG2b/k) was generated by immunization with the ovalbumin coupled peptide Cys-MVGGVVIAT:hybridoma supernatants were used 1:40 for immunoblotting. Protein-G Sepharose-purified monoclonal 13D6 was used for immunostaining. The primary antibodies were detected with biotinylated secondary antibodies and visualized with the avidin–biotin complex method (Vector Laboratories, CA, USA) with diaminobenzidine-HCl as chromogen [41] or processed in a Leica BOND-MAX Automated IHC/ISH Stainer according to the manufacturer's protocol. 3,3′-diaminobenzidine (Liquid DAB + Substrate Chromogen System, Dako) was used as a chromogen to yield brown reaction products. Counterstaining was performed with hematoxylin.

Table 1 List of human autopsy cases

Case number	Age	Sex	Aβ phase	Braak-NFT stage	CERAD score	NIA-AA degree of AD pathology	CAA type	CDR score	Neuropathological diagnosis	PMI	PrP^C-positive neurons (area 36) (%)	PrP^C-positive plaques (area 36) (%)	Co-IP Aβ with PrP^C	Co-IP τ with PrP^C
1	69	m	5	6	2	3	1	1	AD with clinical signs of semantic variant PPA	24	10.46	0	++	+++
2	72	m	5	6	2	3	1	2	AD with clinical signs of primary progressive aphasia (PPA), ARTAG, and cortical and cerebellar microinfarcts	12	5.40	0	++	+++
3	87	m	5	6	2	3	2	2	AD	12	6.25	0	+++	+++
4	76	m	5	5	3	3	1	3	AD	24	8.45	0	++	+++
5	85	m	5	5	2	3	1	2	AD, FTLD TDP type C	48	21.70	0	++	−
6	71	m	5	5	3	3	1	3	AD	12	4.58	0	−	+
7	91	f	3	4	1	2	0	3	AD	n.k.	No paraffin tissue available	No paraffin tissue available	−	−
8	65	m	5	4	3	2	1	3	AD with PSEN1 mutation, and right temporal traumatic brain lesion	12	5.28	1.28	+++	+++
9	82	m	4	4	2	2	1	3	AD with TDP43 pathology and clinical signs of semantic variant PPA and AD	24	16.13	0.33	−	+
10	82	m	4	2	1	1	2	3	AD	12	9.25	0	−	−
11	67	m	4	3	0	2	0	0	p-preAD	13	8.43	0,48	−	−
12	72	f	1	2	0	1	0	0	p-preAD	24	31.48	0.62	−	−
13	77	f	3	2	0	1	0	0	p-preAD	48	16.47	0	−	−
14	73	f	2	1	0	1	0	0	p-preAD	12	6.62	0.63	−	−
15	80	m	2	1	0	1	0	0	p-preAD	48	25.15	0	−	−
16	69	f	0	2	0	0	0	0	Non-AD control with PART	24	21.83	0	−	−
17	68	m	0	1	0	0	0	0	Non-AD control with PART	n.k.	16.33	0	−	−
18	67	m	0	0	0	0	0	0	Non-AD control	n.k.	15.96	0	−	−
19	74	m	0	0	0	0	0	0	Non-AD control	72	12.12	0	−	−

Sections were mounted with Eukitt® or Leica CV mount®. The TG3 anti-τ IgM antibody was visualized with carbocyanine 2-labeled anti-IgM secondary antibodies. Triple-label immunofluorescence was carried out for co-staining with antibodies detecting p-τ (AT8, 1/100 for immunofluorescence; 1H6L6, monoclonal rabbit, 1/500, microwave and formic acid pretreatment, Pierce-Thermo Scientific, MA, USA), Aβ ($Aβ_{17–24}$, 4G8, 1/1000, formic acid pretreatment; $Aβ_{40}$, polyclonal rabbit, 1/100, formic acid pretreatment, IBL, Minneapolis, USA; $Aβ_{42}$, polyclonal rabbit, 1/100, formic acid pretreatment; or $Aβ_{42/43}$, monoclonal rat, 13D6,1/1000, formic acid pretreatment; for characterization of this antibody see Suppl. Figure 1), and PrP^C (6D11). Primary antibodies were detected with carbocyanine 2 (Cy2), Cy3, or Cy5 labeled anti-mouse IgG, anti-rabbit IgG, or anti-rat IgG secondary antibodies. Sections were mounted with Leica CV mount® or ProLong Gold containing DAPI for nuclear counterstaining. When using mouse-derived primary antibodies in mouse tissue, the sections were incubated with non-labeled goat-derived anti-mouse-IgG antibodies or Fab fragments to block staining of intrinsic mouse IgG [90]. Positive and negative controls were included. All tissue sections were viewed with an Olympus BX 51 or a Leica DMLB 2 light microscope. Digital photographs were taken with a Leica DFC7000 T, DC 500, or a Leica DCC 290 camera. Images from triple stained sections were processed with ImageJ (NIH, Bethesda, USA) or CorelPhotopaint 17 (Corel Corporation, Ottawa, Canada). Cy2-labeled signals were pseudo-coded in green, Cy3 in blue, and Cy5 in red.

To test whether PrP^C-positive material contains pathologically folded, proteinase K-resistant PrP^{SC} aggregates, we treated sections from human cases nos. 4 and 8 with proteinase K (Proteinase K—ready to use; DAKO, Glostrup, Denmark) for 2 min before staining with anti-PrP^C (6D11) as described above. These proteinase K-treated sections also served as additional negative control for the PrP^C immunohistochemistry.

Staging and classification of pathology

Mice

The extent of p-τ and Aβ pathology was assessed in analogy to that in the human brain by applying previously published protocols adapted for transgenic mice [44, 87]. For this purpose, p-τ (AT8)- and Aβ (4G8)-stained, sagittally cut brain hemisphere sections covering the cortex, basal ganglia, thalamus, brainstem, and cerebellum were analyzed. Phases of Aβ-plaque deposition (Aβ phases) in APP23xTAU58 and APP51/16xTAU58 mice were determined as follows: phase 1 exhibits only neocortical Aβ plaques, phase 2 shows neocortical and allocortical plaques, phase 3 has additional plaques in the basal ganglia, thalamus, and hypothalamus, phase 4 shows an expansion of plaque pathology into the midbrain and/or the medulla oblongata, and phase 5 exhibits plaques nearly all over the brain including the cerebellum and/or the pons [73, 87]. Due to the different pattern of Aβ pathology in APP48 mice lacking Aβ plaques [1], no staging of Aβ pathology was performed in these mice. NFT distribution was assessed according to a staging system for p-τ pathology in transgenic mice with a neuron-specific promoter by Hurtado et al. [44]: Stage I is characterized by a small number of p-τ-positive neurons, limited to entorhinal region and the isocortical layers II and III, stage II by p-τ-positive neurons in the amygdala, the piriform area, hippocampal CA1 region, or the hypothalamus, stage III by affection of the isocortical layer V and progression of the p-τ pathology into further subfields of the hippocampal formation (CA3 and the dentate gyrus), stage IV by beginning affection of the striatum, prominent p-τ pathology in the hippocampal formation with additional p-τ-positive neurons in the strata radiatum, lucidum and oriens and expansion of p-τ pathology into the midbrain, stage V by the involvement of the layers IV and V into cortical p-τ-pathology, and, finally, stage VI is identified by p-τ pathology in all cortical layers including layer I and severe pathology in neurons of the dentate gyrus. Neuron loss is evident in this stage as well. To assess the entorhinal regions of the mouse lines with significant CA1 p-τ-pathology (APP23xTAU58 and APP51/16xTAU58), sections of the entorhinal cortex level from 5 mice of each of the two mouse lines were stained with anti-p-τ antibodies (AT8).

The percentage of p-τ-positive (AT8-stained) neurons in the frontocentral cortex and in the CA1 region of the hippocampus was determined by counting the number of all neurons in a given reference area, covering 515–1015 frontocentral neurons including all layers or 129–339 CA1 neurons per mouse, and counting the number of the respective p-τ-positive neurons. Neurons were identified based upon their anatomical appearance and their nuclear pattern with a nucleolus. The percentage was calculated as indicated in Suppl. Figure 2a.

To evaluate the extent of co-localization between PrP^C, p-τ, and Aβ in the mouse models, the frontocentral cortex, CA1 and the dentate gyrus were analyzed based on the triple-labeling immunofluorescence with anti-PrP^C (6D11), anti-p-τ (1H6L6), and anti-Aβ (13D6). First, a reference area for each region was identified, covering 68-195 DAPI-positive neurons in the frontocentral cortex, 62–138 in CA1 and 142–570 in the dentate gyrus. Neurons were identified based on their anatomical appearance and their nuclear pattern with a nucleolus. Then, the number of single PrP^C-positive, p-τ-positive, and Aβ-positive neurons as well as the number of neurons with co-localization of PrP^C and p-τ or PrP^C and Aβ was counted. The percentage of the respective positive

neurons from all DAPI-positive neurons was calculated as indicated in Suppl. Figure 2b, c.

To assess the extent of the subcellular co-localization between PrP^C and p-τ, PrP^C + p-τ double positive neurons from APP23xTAU58 (23 neurons), APP51/16xTAU58 (20 neurons), APP48xTAU58 (9 neurons), and TAU58 mice (21 neurons) (cortex, CA1, and dentate gyrus regions) were analyzed with the ImageJ co-localization finder plugin, respectively. Briefly, PrP^C + p-τ double positive neurons were identified and cropped, followed by background removal and analysis with the co-localization finder plugin. The Pearson's correlation coefficient was used as readout.

Human cases

Phases of Aβ plaque deposition in the medial temporal lobe (Aβ-MTL phases) were assessed representing an appropriate estimate for Aβ deposition in the entire brain as previously shown [91, 92]. Braak stages for NFT expansion throughout the brain were determined as previously described based on anti-p-τ stained sections [7, 9]. The frequency of p-τ-positive neuritic plaques was assessed according to the recommendations of the consortium to establish a registry for AD (CERAD) [61]. The National Institute of Aging-Alzheimer Association (NIA-AA) degree of AD pathology was determined according to Hyman et al. [45], based on the Aβ-MTL phase, Braak-NFT stage, and the CERAD score for neuritic plaque pathology. CAA was diagnosed when Aβ deposits were found in the wall of cerebral and/or leptomeningeal blood vessels. The presence of capillary Aβ was employed to distinguish two types of CAA as previously reported [88]: CAA cases exhibiting capillary involvement were assessed as CAA-type 1; CAA cases lacking capillary CAA as CAA-type 2.

The plaque loads for Aβ (4G8)-positive plaques and PrP^C (3F4)-positive plaques were assessed as previously described [73]. In short, the Aβ and PrP^C-plaque loads were determined as the percentage of the area covered by Aβ or PrP^C-positive plaques in a reference area of the temporal neocortex (Brodmann area 36) (size of reference area: ~ 1 mm^2) covered by the respective plaques. The reference area covered all cortical layers. Morphometry was performed using ImageJ image processing and analysis software (National Institutes of Health, Bethesda, MD, USA). The percentage was calculated as indicated in Suppl. Figure 2e, f. The percentage of PrP^C-positive (3F4-stained) neurons in the temporal cortex (area 36) was determined by counting the number of all neurons in a given reference area (ranging from 86 to 356 neurons per case) covering all layers of the temporal neocortex of Brodmann area 36 and counting the number of the respective PrP^C-positive neurons. Neurons were identified based upon their anatomical appearance and their nuclear pattern with a nucleolus. The percentage was calculated as indicated in Suppl. Figure 2d.

Proximity ligation assay

To demonstrate whether PrP^C and $Aβ_{40}$, PrP^C and p-τ, $Aβ_{40}$ and p-τ, as well as $Aβ_{42}$ and PrP^C occur in proximity to one another, i.e., that they are found in a distance of no more than 30–40 nm, we performed a proximity ligation assay [27, 83] in one mouse brain of each line and in one AD case (no. 8) and one non-AD control case with PART (no. 17) [27, 83]. For these experiments, the Duolink® In Situ Orange Starter Kit Mouse/Rabbit (Sigma-Aldrich, Missouri, USA) was used according to the manufacturer's protocol. The principle of this technique is the use of secondary ligands linked to oligonucleotides that can guide circular DNA formation when in less than 30–40 nm distance. This circular DNA is then amplified by rolling-circle amplification and the resulting DNA product is visualized by fluorescence labeled complementary oligonucleotides [27, 83]. Primary antibodies against p-τ (AT8, mouse monoclonal; 1H6L6, rabbit monoclonal), $Aβ_{40}$ (rabbit polyclonal), $Aβ_{42}$ (rabbit polyclonal), and PrP^C (6D11, mouse monoclonal) were used with similar pretreatment and dilutions as previously described (see immunohistochemistry). Anti-human alpha-smooth muscle actin (ACTA2, 1/1000, rabbit polyclonal) and anti-tropomyosin α1 isoform (TM, 1/1000, mouse monoclonal) antibodies, targeting the well-known, physiological protein interaction in smooth muscle cells between actin filaments and tropomyosin, were used in a cortex section of case no. 8 as positive (blood vessels with smooth muscle cells) and intrinsic negative control (brain parenchyma) for proximity labeling. The following mouse/rabbit antibody combinations were used: (1) 1H6L6–6D11; (2) $Aβ_{40}$–6D11; (3) $Aβ_{42}$–6D11; (4) $Aβ_{40}$–AT8; (5) ACTA2–TM. This analysis was carried out only for demonstration purposes to confirm the findings observed by immunofluorescence triple labeling.

Biochemistry

Protein extraction from frozen forebrain hemispheres of 6-month-old APP23xTAU58 ($n = 6$), APP51/16xTAU58 ($n = 6$), APP48xTAU58 ($n = 6$), and TAU58 mice ($n = 6$) as well as from human frozen brain samples from the entorhinal cortex of cases 1–19 was carried out as previously described [73, 74]. Briefly, fresh-frozen brain tissue samples (0.4 g) were homogenized in 2 ml of 0.32 M sucrose dissolved in Tris-buffered saline (TBS) containing a protease and phosphatase inhibitor-cocktail (Complete and PhosSTOP, Roche, Mannheim, Germany) with Micropestle

(Eppendorf, Hamburg, Germany) followed by sonication. The homogenate was centrifuged for 30 min at 14,000×*g* at 4 °C. The supernatant (S1) containing both the soluble and dispersible fraction was kept for further ultracentrifugation. The pellet (P1) containing the membrane-associated and the insoluble, plaque-associated fraction was resuspended in 2% SDS. Ultracentrifugation of the supernatant S1 at 175,000×*g* was used to separate the soluble, i.e., the supernatant after ultracentrifugation (S2), from the dispersible fraction, i.e., the resulting pellet (P2). The pellet P2 with the dispersible fraction was resuspended in TBS.

The SDS-resuspended pellet P1 was centrifuged at 14,000×*g* and the supernatant (S3) was kept as membrane-associated SDS-soluble fraction. The pellet (P3) that remained was dissolved in 70% formic acid and dried in a vacuum centrifuge (Vacufuge, Eppendorf, Hamburg, Germany) and reconstituted in 100 µl of 2× LDS (lithium dodecyl sulfate) sample buffer (Life Technologies, Carlsbad, CA, USA) followed by heating at 70 °C for 5 min. The resultant sample was considered as insoluble, only formic acid-soluble, fraction [59]. The total protein amounts of soluble, dispersible, and membrane-associated fractions were determined using BCA Protein Assay (Bio-Rad, Hercules, CA, USA).

Protein extraction from human tissue was carried out in analogy to that for the mouse homogenates, with the following modifications. Initially, 50 mg of entorhinal cortex tissue were homogenized in 1 mL of cold H buffer (10 mM Tris, 0.8 M NaCl, 10% sucrose, pH 7.4) containing protease and phosphatase inhibitors followed by sonication. The following steps were performed as previously described for the mice, with an additional incubation step with 1% sarkosyl for 1 h at 37 °C before ultracentrifugation of S1 to isolate sarkosyl-insoluble tau aggregates (P2) from the sarkosyl-soluble fraction (S2).

For immunoprecipitation *(IP)* of Aβ oligomers and protofibrils/fibrils, 200 µl of the native soluble and dispersible fractions from the mouse brain lysates were incubated with 1 µl A11 antibodies [50] (A11, Millipore, Temecula,CA, USA; 1 µl/200 µl lysate) against non-fibrillar oligomers, or 5 µl B10AP antibody fragments [37] (B10AP; 1 µl/200 µl lysate) for precipitation of protofibrils and fibrils. 50 µl of protein G Microbeads (Miltenyi Biotec, Bergisch-Gladbach, Germany) were added to the mixture and incubated overnight at 4 °C. The mixture was then passed through µColumns, which separate the microbeads by retaining them in the column, while the rest of the lysate flows through. After one mild washing step with 1× TBS at pH 7.4, the microbead-bound proteins were eluted with 95 °C heated 1X LDS sample buffer (Life Technologies, Carlsbad, CA, USA).

For IP of PrP^C, Aβ, and p-τ, respectively, 130 µl of the native soluble (S2) and dispersible fractions (P2) from the mouse brain lysates or sarkosyl-insoluble fractions (P2) from human brain lysates were incubated with 1.2 µg of either anti-PrP^C (6D11), anti-p-τ (PHF1) or anti-$Aβ_{1–17}$ (6E10) antibodies. 35 µl of magnetic microbeads (Miltenyi Biotec) were added to the mixture and incubated for 2 h at 4 °C. The mixture was then passed through the µColumns and washed 4× with high salt buffer (500 mM NaCl, 50 mM Tris HCl, pH 8.0) and 1× with low salt buffer (50 mM Tris HCl, pH 8.0). Finally, microbead-bound proteins were eluted with 95 °C heated 1× LDS sample buffer.

For SDS-PAGE, soluble (S2), dispersible (P2), membrane-associated (SDS-soluble; S3), insoluble, only formic acid-soluble (P3) fractions from mouse brain homogenates, and sarkosyl-insoluble (P2) fractions from human brain lysates and IP eluates (50 µg total protein) were electrophoretically resolved in a precast NuPAGE 4–12% Bis–Tris gel system (Life Technologies, Carlsbad, CA, USA). Proteins were transferred onto Nitrocellulose membrane and membranes were boiled in 1× PBS for 5 min. The protein load was controlled either by Ponceau S staining (C4, 1/1000, Santa Cruz Biotechnology, Santa Cruz, CA, USA) or by MemCode reversible protein stain kit (Pierce, Rockford, IL, USA) prior to immunoblotting. Then, membranes were blocked in 5% non-fat dry milk (diluted in PBS-T) for 1 h.

For detection of Aβ, APP_{CTFs}, PrP^C, and p-τ by western blotting, antibodies raised against p-τ (PHF1, 1/2000; AT8, 1/1000), $Aβ_{1–17}$ (6E10, 1/4000), $Aβ_{40}$ (IBL-polyclonal, 1/1000), APP_{CTF} (1/4000, anti-rabbit monoclonal, Millipore, USA), and PrP^C (6D11, 1:1000) were used. Blots were incubated with chemiluminescent ECL detection system (Supersignal Dura Western system, ThermoScientific-Pierce, Waltham, MA, USA) or Luminata Forte Western HRP substrate (Merck Millipore, Billerica, Massachusetts, USA) and acquired using either ECL Hyperfilm (GE Healthcare, Buckinghamshire, UK) or CCD imager Image Quant LAS 4000 (GE Healthcare, Buckinghamshire, UK). In the event that the available brain homogenates did not allow multiple blots after immunoprecipitation, the membranes were consecutively stripped. After detection, membranes were washed in PBS-T for 5 min and incubated for 10 min in Restore Western Blot Stripping Buffer (Life Technologies, Carlsbad, CA, USA), followed by another 5 min wash in PBS-T. Then, membranes were blocked and incubated with another primary antibody as described above. To avoid inconclusive results due to the use of the stripping method, we always used primary antibodies against different proteins in consecutive stripping cycles. This way, the specific protein bands could be differentiated from the previous staining of the membrane.

Because Aβ aggregates readily dissociate into monomers and small oligomers, such as dimers, trimers, or Aβ*56 in the presence of SDS-containing buffers [75, 104], we analyzed differences among Aβ-monomer bands that indicate

changes in the protein levels of precipitated Aβ aggregates densitometrically using ImageJ software (NIH, Bethesda, MD, USA). This method allowed the semiquantitative assessment of Aβ in a given fraction [73]. Briefly, the X-ray films were scanned. Image colors were inverted or the images acquired by CCD imager were exported as 8-bit grayscale TIFF-files. The relative protein levels of the monomer bands were measured as integrated density values for each lane [80].

ELISA: For determination of the levels of total τ and p-τ in brain homogenates of 28 mice including APP23 ($n=2$), APP51/16 ($n=2$), APP48 ($n=2$), TAU 58 ($n=6$), APP23x-TAU58 ($n=4$), APP51/16xTAU58 ($n=6$), and APP48x-TAU58 mice ($n=6$), ELISA measurements were carried out with an MSD® MULTI-SPOT p-τ (Thr231)/total τ assay on an MSD-ELISA-reader (Meso Scale Diagnostics, Rockville, MD, USA). All samples were measured in duplicates. The mean values of the calculated concentrations were used for further analysis of the ELISA-data.

Pull-down assay

To clarify whether the PrP^C protein is primarily able to interact physically with Aβ and p-τ, we performed a pull-down assay using recombinant his-tagged PrP^C (amino acids 23–231 fused to a His Tag® sequence and expressed in E. coli, Merck Millipore Billerica, Massachusetts, USA) as bait protein. Briefly, 10 µg of his-tagged PrP^C were incubated with 25 µl of nickel chelate beads (Ni–NTA resin, Bio-Rad) for 45 min at 4 °C. Then, nickel chelate beads bound to his-tagged PrP^C were incubated with either 5 µg of synthetic $Aβ_{40}$ (AnaSpec), $Aβ_{42}$ (AnaSpec), or with 35 µg of p-τ-rich human AD brain extract (case no. 2) for 2 h at 4 °C. Nickel chelate beads without his-tagged PrP^C were also incubated with purified $Aβ_{40}$ and $Aβ_{42}$ or human AD brain extract as negative controls. The beads were finally washed 3x in His wash buffer (50 mM NaH_2PO_4 pH 8.0, 300 mM NaCl, and 20 mM imidazole), and eluted by incubation with His elution buffer for 10 min (the same buffer with 250 mM imidazole). The samples were further analyzed by SDS-PAGE and western blot as described before (see "Biochemistry").

Statistical analysis

Statistical analysis was carried out with IBM-SPSS 24. To compare the percentages of abnormal τ-protein containing neurons, the percentages of PrP^C + p-τ double positive neurons, PrP^C + Aβ double positive neurons, and levels of Aβ measured by quantifying the 4 kDa bands among the different mouse lines at 6 months of age, we used the Kruskal–Wallis *H* test with the Bonferroni correction for multiple testing. To clarify whether there is an association between Aβ and PrP^C-plaque loads or the percentage of PrP^C-positive neurons in the temporal neocortex with the AD disease stage (non-AD–p-preAD–AD), the Braak-NFT stage, the amyloid phase, the CERAD score for neuritic plaque pathology, and the degree of AD pathology [45], we used linear regression models. In a first step, only one independent variable (Aβ plaque load, PrP^C-plaque load, or percentage of PrP^C-positive neurons) was integrated in the model term. In a second step, for those models showing a significant effect of the independent variable, age and sex were added as further independent variables into the model term. The sign test was used to compare Aβ and PrP^C-plaque loads in the human cases.

Results

Acceleration of p-τ-pathology spreading in APP23xTAU58 and APP51/16xTAU58 mice

To address the question whether Aβ has impact on p-τ-pathology, especially on its spreading into non-affected brain regions, we studied three double-transgenic mouse models. We crossed TAU58 mice with three different mouse lines that transgenically produce Aβ: (1) APP23 mice overexpressing human APP carrying the Swedish mutation (KM → NL) [85], (2) APP51/16 mice expressing human wild-type APP [73], and (3) APP48 mice expressing a proenkephalin signal peptide coupled to $Aβ_{42}$, releasing $Aβ_{42}$ into the endoplasmic reticulum and the Golgi apparatus independently of APP and forming exclusively intracellular $Aβ_{42}$ aggregates [1]. TAU58 mice lacking transgenic Aβ production were used as controls. All mice were analyzed at 6 months of age.

Using immunohistochemistry with antibodies directed against p-τ, we found accelerated spreading of p-τ-pathology in APP23xTAU58 and APP51/16xTAU58 mice compared to TAU58 mice but not in APP48xTAU58 mice. p-τ was found in neurons of the brainstem and the neocortex of all four mouse lines (Fig. 1a–d). In the frontocentral cortex, the percentage of p-τ-positive neurons did not differ significantly between APP23xTAU58 and TAU58 mice, whereas APP51/16xTAU58 and APP48xTAU58 mice showed lower percentages of p-τ-expressing neurons than APP23xTAU58 and TAU58 mice (Fig. 1e, Table 2b). p-τ-positive hippocampal neurons in the CA1 region were also found in all APP23xTAU58 and APP51/16xTAU58 mice but only in 44.44% of the TAU58 mice and in 36.36% of the APP48xTAU58 mice (Fig. 1f–i), pointing to an accelerated expansion, i.e., spreading of p-τ into the CA1 region of APP23xTAU58 and APP51/16xTAU58 mice. The percentage of p-τ exhibiting neurons in the hippocampal region CA1 was higher in APP23xTAU58 and APP51/16xTAU58 mice compared to TAU58 mice (Fig. 1j, Table 2a). The

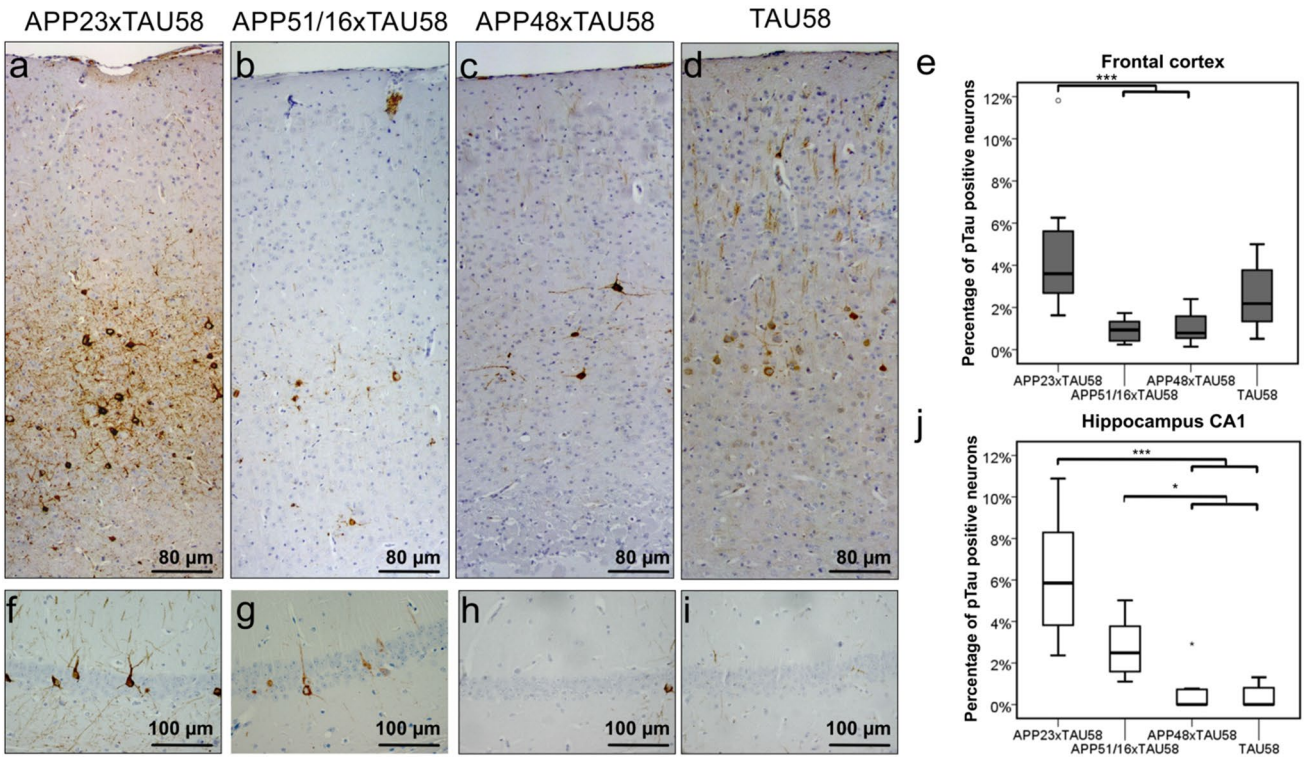

Fig. 1 Spreading of p-τ pathology in APP23xTAU58, APP51/16xTAU58, APP48xTAU58, and TAU58 mice. p-τ pathology in the frontocentral cortex (**a–d**) and hippocampal sector CA1 (**e–h**) in APP23xTAU58 (**a**, **f**), APP51/16xTAU58 (**b**, **g**), APP48xTAU58 (**c**, **h**), and TAU58 mice (**d**, **i**). p-τ is stained with the AT8-antibody. In the frontocentral cortex, the neuropil staining was most prominent in APP23xTAU58 mice (**a**). Significant p-τ pathology in the hippocampal sector CA1 was restricted to APP23xTAU58 and APP51/16xTAU58 mice (**f**, **g**), whereas p-τ-positive neurons were virtually lacking in the CA1 sector of APP48xTAU58 and TAU58 mice (**h**, **i**). **e** Percentages of p-τ exhibiting neurons in the frontocentral cortex of APP23xTAU58, APP51/16xTAU58, APP48xTAU58, and TAU58 mice. The percentages of p-τ-positive neurons in TAU58 mice did not significantly differ from that in APP23xTAU58, APP51/16xTAU58, and APP48xTAU58 mice. **j** Percentage of p-τ exhibiting neurons in the hippocampal CA1 sector of APP23xTAU58, APP51/16xTAU58, APP48xTAU58, and TAU58 mice. In the hippocampal sector CA1, the percentage of p-τ exhibiting neurons is higher in APP23xTAU58 and APP51/16xTAU58 mice than in TAU58 mice, whereas the percentage of p-τ-positive neurons in CA1 did not differ between APP48xTAU58 and TAU58 mice. Kruskal–Wallis *H* test corrected for multiple testing by the Bonferroni method: $*p<0.05$, $***p<0.001$; for detailed statistical analysis, see Table 2a, b. **e**, **j** $n=18$ (TAU58); 13 (APP23xTAU58); 8 (APP51/16xTAU58); 11 (APP48xTAU58)

distribution of p-τ pathology in the mice fit with the pattern reported by the staging system of Hurtado et al. [44], ranged between stages 1 and 3, and demonstrated increased stages of p-τ pathology in APP23xTAU58 mice in comparison with TAU58 mice indicating an aggravated spreading of p-τ pathology in APP23xTAU58 mice. APP51/16xTAU58 mice showed a trend towards higher Hurtado stages compared to TAU58 mice as seen when not correcting for multiple testing (Table 2c).

p-τ pathology in all mouse lines contained only 4-repeat τ-lesions, exhibiting the phosphoepitopes $pSer^{202}/pThr^{205}$ (AT8), $pSer^{396}/pSer^{404}$ (PHF1) of τ, the conformational epitope TG3, and argyrophilic NFTs detected with the Gallyas silver staining method (Fig. 1, Suppl. Figures 3–5). 3-repeat τ was observed only in its physiological expression site in cells of the dentate gyrus subgranular zone (Suppl.-Figure 3a–d) [60]. The concentration of total τ-protein and p-τ in forebrain homogenates among the four different mouse lines with a TAU58 background did not vary significantly as determined by ELISA (Suppl. Figure 6). Thus, histopathological spreading of p-τ pathology in APP23xTAU58 and APP51/16xTAU58 mice was not associated with a detectable general increase in p-τ or total τ-protein content in the brain of the 6-month-old mice.

To clarify whether accelerated spreading of p-τ pathology in APP23xTAU58 and APP51/16xTAU58 mice was related to a specific pool of Aβ aggregates, we performed western blot analysis of soluble, dispersible, membrane-associated, and formic acid-soluble Aβ from forebrain homogenates. At the age of 6 months, APP23xTAU58 mice had the highest levels of soluble and dispersible Aβ (Fig. 2a, b). The difference in soluble Aβ was significant when comparing APP23xTAU58 with TAU58 mice but not when comparing APP51/16xTAU58 and APP48xTAU58

Table 2 Statistical analysis

(**a**) Comparison of the percentages of abnormal τ-protein containing neurons among 6-month-old APP23xTAU58, APP51/16xTAU58, APP48xTAU58, and TAU58 mice in the CA1 regions of the hippocampus. Kruskal-Wallis H-test corrected for multiple testing by the Bonferroni correction. n = 18 (TAU58); 13 (APP23x-TAU58); 8 (APP51/16xTAU58); 11 (APP48xTAU58)

		p	p (not corrected)
APP23xTAU58	APP51/16xTAU58	1.000	0.181
APP23xTAU58	APP48xTAU58	>0.001	>0.001
APP23xTAU58	TAU58	>0.001	>0.001
APP51/16xTAU58	APP48xTAU58	0.021	0.004
APP51/16xTAU58	TAU58	0.012	0.002
APP48xTAU58	TAU58	1.000	0.906

(**b**) Comparison of the percentages of abnormal τ-protein containing neurons among 6-month-old APP23xTAU58, APP51/16xTAU58, APP48xTAU58, and TAU58 mice in the frontocentral cortex. Kruskal-Wallis H-test corrected for multiple testing by the Bonferroni correction. n = 18 (TAU58); 13 (APP23x-TAU58); 8 (APP51/16xTAU58); 11 (APP48xTAU58)

		p	p (not corrected)
APP23xTAU58	APP51/16xTAU58	>0.001	>0.001
APP23xTAU58	APP48xTAU58	>0.001	>0.001
APP23xTAU58	TAU58	0.251	0,042
APP51/16xTAU58	APP48xTAU58	1.000	0.711
APP51/16xTAU58	TAU58	0.055	0.009
APP48xTAU58	TAU58	0.087	0.014

(**c**) Comparison of the stages of the distribution of abnormal τ-protein containing neurons in 6-month-old APP23xTAU58, APP51/16xTAU58, APP48xTAU58, and TAU58 mice according to Hurtado el al. [14]. Kruskal-Wallis H-test corrected for multiple testing by the Bonferroni correction. n = 18 (TAU58); 13 (APP23x-TAU58); 8 (APP51/16xTAU58); 11 (APP48xTAU58)

		p	p (not corrected)
APP23xTAU58	APP51/16xTAU58	1.000	0.340
APP23xTAU58	APP48xTAU58	>0.001	>0.001
APP23xTAU58	TAU58	>0.001	>0.001
APP51/16xTAU58	APP48xTAU58	0.011	0.002
APP51/16xTAU58	TAU58	0.057	0.009
APP48xTAU58	TAU58	1.000	0.361

(**d**) Comparison of the levels of soluble Aβ in the brain of 6-month-old APP23xTAU58, APP51/16xTAU58, APP48xTAU58, and TAU58 mice. Kruskal-Wallis H-test corrected for multiple testing by the Bonferroni correction. n = 6 (for each group).

		p	p (not corrected)
APP23xTAU58	APP51/16xTAU58	0.850	0.142
APP23xTAU58	APP48xTAU58	0.003	0.001
APP23xTAU58	TAU58	0.001	>0.001
APP51/16xTAU58	APP48xTAU58	0.273	0.045
APP51/16xTAU58	TAU58	0.096	0.016
APP48xTAU58	TAU58	1.000	0.683

Table 2 (continued)

(**e**) Comparison of the levels of dispersible Aβ in the brain of 6-month-old APP23xTAU58, APP51/16xTAU58, APP48xTAU58, and TAU58 mice. Kruskal-Wallis H-test corrected for multiple testing by the Bonferroni correction. n = 6 (for each group).

		p	p (not corrected)
APP23xTAU58	APP51/16xTAU58	0.300	0.050
APP23xTAU58	APP48xTAU58	0.397	0.066
APP23xTAU58	TAU58	>0.001	>0.001
APP51/16xTAU58	APP48xTAU58	1.000	0.903
APP51/16xTAU58	TAU58	0.148	0.025
APP48xTAU58	TAU58	0.107	0.018

(**f**) Comparison of the levels of membrane-association, SDS-soluble Aβ in the brain of 6-month-old APP23xTAU58, APP51/16xTAU58, APP48xTAU58, and TAU58 mice. Kruskal-Wallis H-test corrected for multiple testing by the Bonferroni correction. n = 6 (for each group).

		p	p (not corrected)
APP23xTAU58	APP51/16xTAU58	1.000	0.935
APP23xTAU58	APP48xTAU58	1.000	0.870
APP23xTAU58	TAU58	0.015	0.003
APP51/16xTAU58	APP48xTAU58	1.000	0.935
APP51/16xTAU58	TAU58	0.020	0.003
APP48xTAU58	TAU58	0.026	0.004

(**g**) Comparison of the levels of formic acid-soluble Aβ in the brain of 6-month-old APP23xTAU58, APP51/16xTAU58, APP48xTAU58, and TAU58 mice. Kruskal-Wallis H-test corrected for multiple testing by the Bonferroni correction. n = 6 (for each group).

		p	p (not corrected)
APP23xTAU58	APP51/16xTAU58	0.615	0.102
APP23xTAU58	APP48xTAU58	1.000	0.253
APP23xTAU58	TAU58	0.012	0.002
APP51/16xTAU58	APP48xTAU58	0.033	0.006
APP51/16xTAU58	TAU58	0.850	0.142
APP48xTAU58	TAU58	>0.001	>0.001

(**h**) Comparison of the levels of dispersible Aβ oligomers immunoprecipitated with A11 antibodies in the brain of 6-month-old APP23xTAU58, APP51/16xTAU58, APP48xTAU58, and TAU58 mice. Kruskal-Wallis H-test corrected for multiple testing by the Bonferroni correction. n = 6 (for each group).

		p	p (not corrected)
APP23xTAU58	APP51/16xTAU58	0.054	0.009
APP23xTAU58	APP48xTAU58	0.918	0.153
APP23xTAU58	TAU58	>0.001	>0.001
APP51/16xTAU58	APP48xTAU58	1.000	0.236
APP51/16xTAU58	TAU58	0.565	0.094
APP48xTAU58	TAU58	0.026	0.004

with TAU58 mice (Fig. 2a, Table 2d). There was a tendency for more soluble Aβ in APP51/16xTAU58 mice than in TAU58 mice but no significant increase when adjusting the p values for multiple testing (Fig. 2a; Table 2d). As such, these results indicate an association of increased levels of soluble Aβ with spreading of p-τ pathology. For dispersible Aβ, only the difference between APP23x-TAU58 and TAU58 mice was significant. There was a

Table 2 (continued)

(**i**) Comparison of the levels of dispersible Aβ protofibrils and fibrils immunoprecipitated with B-10 antibody fragments in the brain of 6-month-old APP23xTAU58, APP51/16xTAU58, APP48xTAU58, and TAU58 mice. Kruskal-Wallis H-test corrected for multiple testing by the Bonferroni correction. n = 6 (for each group).

		p	p (not corrected)
APP23xTAU58	APP51/16xTAU58	0.022	0.004
APP23xTAU58	APP48xTAU58	0.991	0.164
APP23xTAU58	TAU58	>0.001	>0.001
APP51/16xTAU58	APP48xTAU58	0.785	0.131
APP51/16xTAU58	TAU58	0.850	0.142
APP48xTAU58	TAU58	0.014	0.003

(**j**) Comparison of the percentage of double positive PrP^C/p-τ neurons in the brain of 6-month-old APP23xTAU58, APP51/16xTAU58, APP48xTAU58, and TAU58 mice. Kruskal-Wallis H-test corrected for multiple testing by the Bonferroni correction. n = 6 (APP23xTAU58); n = 7 (APP51/16xTAU58); n = 5 (APP48xTAU58); n = 8 (TAU58).

Frontocentral cortex

		p	p (not corrected)
APP23xTAU58	APP51/16xTAU58	1.000	0.884
APP23xTAU58	APP48xTAU58	0.036	0.006
APP23xTAU58	TAU58	0.485	0,081
APP51/16xTAU58	APP48xTAU58	0.041	0.007
APP51/16xTAU58	TAU58	0.575	0.096
APP48xTAU58	TAU58	1.000	0.205

Hippocampus CA1

		p	p (not corrected)
APP23xTAU58	APP51/16xTAU58	1.000	0.572
APP23xTAU58	APP48xTAU58	1.000	0.423
APP23xTAU58	TAU58	0.036	0.006
APP51/16xTAU58	APP48xTAU58	1.000	0.770
APP51/16xTAU58	TAU58	0.143	0.024
APP48xTAU58	TAU58	0.478	0.080

Dentate gyrus

		p	p (not corrected)
APP23xTAU58	APP51/16xTAU58	1.000	0.850
APP23xTAU58	APP48xTAU58	0.017	0.003
APP23xTAU58	TAU58	0.214	0.036
APP51/16xTAU58	APP48xTAU58	0.007	0.001
APP51/16xTAU58	TAU58	0.100	0.017
APP48xTAU58	TAU58	1.000	0.242

tendency for more dispersible Aβ in APP51/16xTAU58 and APP48xTAU58 than in TAU58 mice when not correcting statistical analysis for multiple testing (Fig. 2b; Table 2e). Membrane-associated Aβ was found increased in APP23xTAU58, APP51/16xTAU58, and APP48xTAU58 mice in comparison to TAU58 mice (Fig. 2c, Table 2f). Accordingly, the presence of dispersible and membrane-associated Aβ in APP48xTAU58 mice showing no exaggeration of p-τ-spreading does not argue for a direct effect of these forms of Aβ aggregates on p-τ pathology propagation, but do not exclude that specifically APP-derived or soluble Aβ-derived forms of dispersible and membrane-associated Aβ may be relevant in this process. Formic acid-soluble Aβ aggregates were more prevalent in APP23xTAU58 and APP48xTAU58 mice than in TAU58 mice (Fig. 2d; Table 2g). Therefore, it does not seem to

Table 2 (continued)

(**k**) Comparison of the percentage of double positive PrP^C/Aβ neurons in the brain of 6-month-old APP23xTAU58, APP51/16xTAU58, APP48xTAU58, and TAU58 mice. Kruskal-Wallis H-test corrected for multiple testing by the Bonferroni correction. n = 6 (APP23xTAU58); n = 7 (APP51/16xTAU58); n = 5 (APP48xTAU58); n = 8 (TAU58).

Frontocentral cortex

		p	p (not corrected)
APP23xTAU58	APP51/16xTAU58	1.000	1.000
APP23xTAU58	APP48xTAU58	>0.001	>0.001
APP23xTAU58	TAU58	1.000	1.000
APP51/16xTAU58	APP48xTAU58	>0.001	>0.001
APP51/16xTAU58	TAU58	1.000	1.000
APP48xTAU58	TAU58	>0.001	>0.001

Hippocampus CA1

		p	p (not corrected)
APP23xTAU58	APP51/16xTAU58	1.000	1.000
APP23xTAU58	APP48xTAU58	>0.001	>0.001
APP23xTAU58	TAU58	1.000	1.000
APP51/16xTAU58	APP48xTAU58	>0.001	>0.001
APP51/16xTAU58	TAU58	1.000	1.000
APP48xTAU58	TAU58	>0.001	>0.001

Dentate gyrus

		p	p (not corrected)
APP23xTAU58	APP51/16xTAU58	1.000	1.000
APP23xTAU58	APP48xTAU58	>0.001	>0.001
APP23xTAU58	TAU58	1.000	1.000
APP51/16xTAU58	APP48xTAU58	>0.001	>0.001
APP51/16xTAU58	TAU58	1.000	1.000
APP48xTAU58	TAU58	>0.001	>0.001

(l) Linear regression analysis of the percentage of PrP^C-positive neurons in the human brain samples as independent variable in its relation to the disease stage (non-AD, p-preAD, AD), CDR-score, NIA-AA degree of AD, Aβ phase, Braak-NFT stage, CERAD neuritic plaque score, and Aβ plaque load as respective dependent variables. n = 18.

Dependent variable	**p**	**β**
Disease stage	0.081	
CDR	0.038	-0.491
NIA-AA	0.062	
Aβ phase	0.019	-0.546
Braak-NFT stage	0.084	
CERAD	0.023	-0.523
Aβ plaque load	0.112	

be likely that insoluble, only formic acid-soluble, aggregates play a major role in exaggerating p-τ-spreading. Immunoprecipitation with A11 antibodies and B10AP-antibody fragments showed increased levels of dispersible Aβ oligomers, protofibrils and fibrils in APP23xTAU58 and APP48xTAU58 mice compared with TAU58 mice. APP51/16xTAU58 mice showed no difference in the amount of dispersible Aβ oligomers, protofibrils, and fibrils in comparison with TAU58 mice. Differences in the amount of soluble A11-precipitated Aβ oligomers and B10AP-precipitated Aβ protofibrils and fibrils were not apparent (Suppl. Figure 8, Table 2h). Thus, extracellular, dispersible Aβ oligomers, protofibrils, or fibrils may be potentially relevant for p-τ pathology spreading in

Table 2 (continued)

(m) Linear regression analysis of the percentage of PrP^C-positive neurons in the human brain samples as independent variable controlled by age and sex as additional independent variables in its relation to the CDR-score, Aβ phase, and CERAD neuritic plaque score as respective dependent variables. n = 18.

Dependent variable	p	β
CDR	0.069	
Aβ phase	0.027	-0.534
CERAD	0.085	

(n) Linear regression analysis of the Aβ plaque loads and the PrP^C plaque loads in the human brain samples as independent variable in its relation to the disease stage (non-AD, p-preAD, AD), CDR-score, NIA-AA degree of AD, Aβ phase, Braak-NFT stage, CERAD neuritic plaque score, and Aβ plaque load as respective dependent variables. n = 18.

	Aβ plaque load		PrP^C plaque load	
Dependent variable	**p**	**β**	**p**	**β**
Disease stage	0.021	0.540	0.588	
CDR	0.293		0.718	
NIA-AA	0.004	0.650	0.979	
Aβ phase	0.002	0.688	0.678	
Braak-NFT stage	0.005	0.636	0.887	
CERAD	0.054		0.675	
Aβ plaque load	n.a.		0.554	

(o) Linear regression analysis of the Aβ plaque loads in the human brain samples as independent variable controlled by age and sex as additional independent variables in its relation to the CDR-score, Aβ phase, and CERAD neuritic plaque score as respective dependent variables. n = 18.

	Aβ plaque load	
Dependent variable	**p**	**β**
Disease stage	0.015	0.510
NIA-AA	0.002	0.793
Aβ phase	0.001	0.872
Braak-NFT stage	0.005	0.724

Kruskal–Wallis *H* test corrected for multiple testing by the Bonferroni correction

APP23xTAU58 mice, whereas intracellular Aβ oligomers, protofibrils, and fibrils in APP48xTAU58 mice do not.

Only one out of ten APP23xTAU58 mice showed one single plaque in the neocortex (= Aβ phase 1) consistent with previously published findings in the respective APP-single transgenic mice [73] of the same age. The other mouse lines did not exhibit plaques (= Aβ phase 0). Cerebral amyloid angiopathy was not observed in the 6-month-old mice.

PrP^C interacts with dispersible Aβ/APP_{CTF} and p-τ in transgenic mice

To further understand whether Aβ can induce cross seeding of p-τ [97] or binds to a protein associated with Aβ/p-τ pathology, such as PrP^C [53, 63], we performed co-immunoprecipitation experiments. First, we determined the input levels of p-τ, PrP^C, Aβ, and APP by western blot analysis of the soluble and dispersible fractions [14, 57]. Here, soluble and dispersible p-τ bands were more prominent in APP23xTAU58 and APP51/16xTAU58 mice compared to APP48xTAU58 and TAU58 mice (Fig. 3a). PrP^C was detected in all four mouse lines with APP48xTAU58 mice exhibiting slightly less strong bands than the other three mouse lines (Fig. 3a). Due to the genetic background of the APP23xTAU58 and APP51/16xTAU58 mice with APP overexpression, APP and its cleavage products CTFs and $Aβ_{40}$ were detected. APP48xTAU58 and TAU58 showed lower levels of APP, reflecting its physiological expression (Fig. 3b). Immunoprecipitation experiments in APP23xTAU58 and APP51/16xTAU58 mice revealed

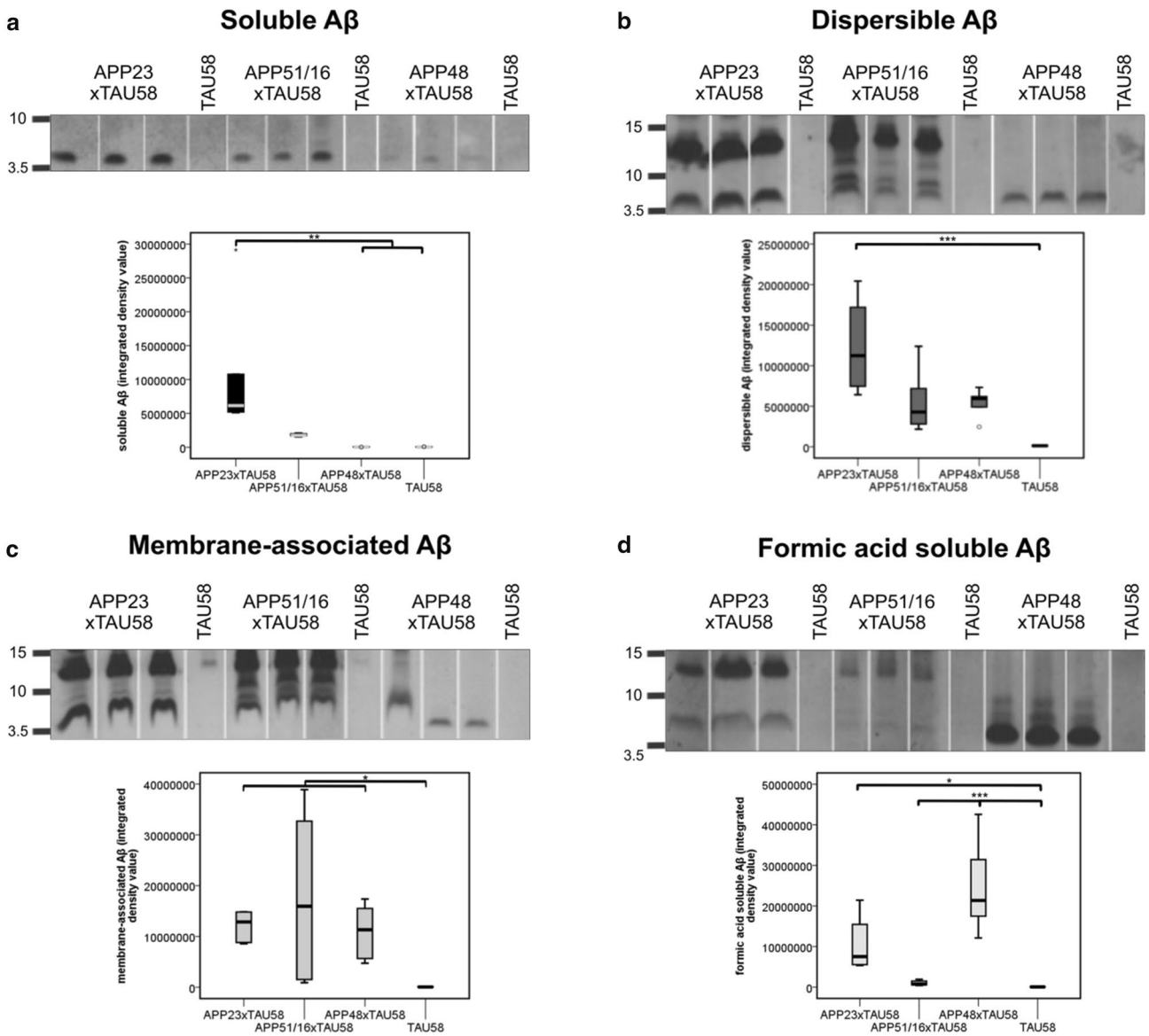

Fig. 2 Levels of soluble, dispersible, membrane-associated, and formic acid/soluble Aβ in APP23xTAU58, APP51/16xTAU58, APP48xTAU58, and TAU58 mice. Western blot analysis with antibodies against $A\beta_{1-17}$ (6E10; $n=6$/group) showed that APP23xTAU58 mice exhibited the highest levels of soluble Aβ (**a**, **b**). APP51/16xTAU58 mice had slightly higher levels of soluble Aβ than TAU58 mice (**a**). APP23xTAU58, APP51/16xTAU58 and APP48xTAU58 mice showed higher levels of dispersible Aβ than TAU58 mice (**b**). Nearly similar amounts of membrane-associated Aβ were observed in APP23xTAU58, APP51/16xTAU58, and APP48xTAU58 mice. TAU58 mice showed less (**c**). Formic acid-soluble Aβ occurred in APP48xTAU58 and APP23xTAU58 mice. APP51/16xTAU58 and TAU58 mice contained only negligible amounts (**d**). Kruskal–Wallis *H* test corrected for multiple testing with the Bonferroni method: $*p<0.05$, $**p<0.01$, $***p<0.001$; (see Table 2d–g). Uncropped blots are provided in Suppl. Fig. 7

higher levels of co-immunoprecipitated p-τ and PrP^C in the dispersible fraction, after precipitating with anti-$A\beta_{1-17}$ (6E10) antibodies, than in TAU58 and APP48xTAU58 mice (Fig. 3c). Aβ in the soluble fraction was bound neither to p-τ nor to PrP^C (Fig. 3c). In the dispersible fraction, immunoprecipitation with anti-p-τ (PHF-1) and anti-PrP^C (6D11) antibodies revealed co-immunoprecipitation of $A\beta_{40}$, APP, APP_{CTF}, and PrP^C or p-τ, respectively, in APP23xTAU58 mice but not in the other mouse lines. In APP51/16xTAU58 mice, APP and APP_{CTF} were also co-immunoprecipitated with p-τ and PrP^C. Only PrP^C and traces of APP were co-immunoprecipitated with p-τ or PrP^C in TAU58 and APP48xTAU58 mice (Fig. 3d, e). Two sets of triple label immunohistochemistry have been performed. When using anti-PrP^C (6D11), anti-p-τ (1H6L6), and anti-$A\beta_{42/43}$ (13D6) antibodies, double labeling of PrP^C and p-τ was seen in a subset of the neurons in the CA1 region (Fig. 4a–h, r), the frontal cortex (Fig. 4q), and

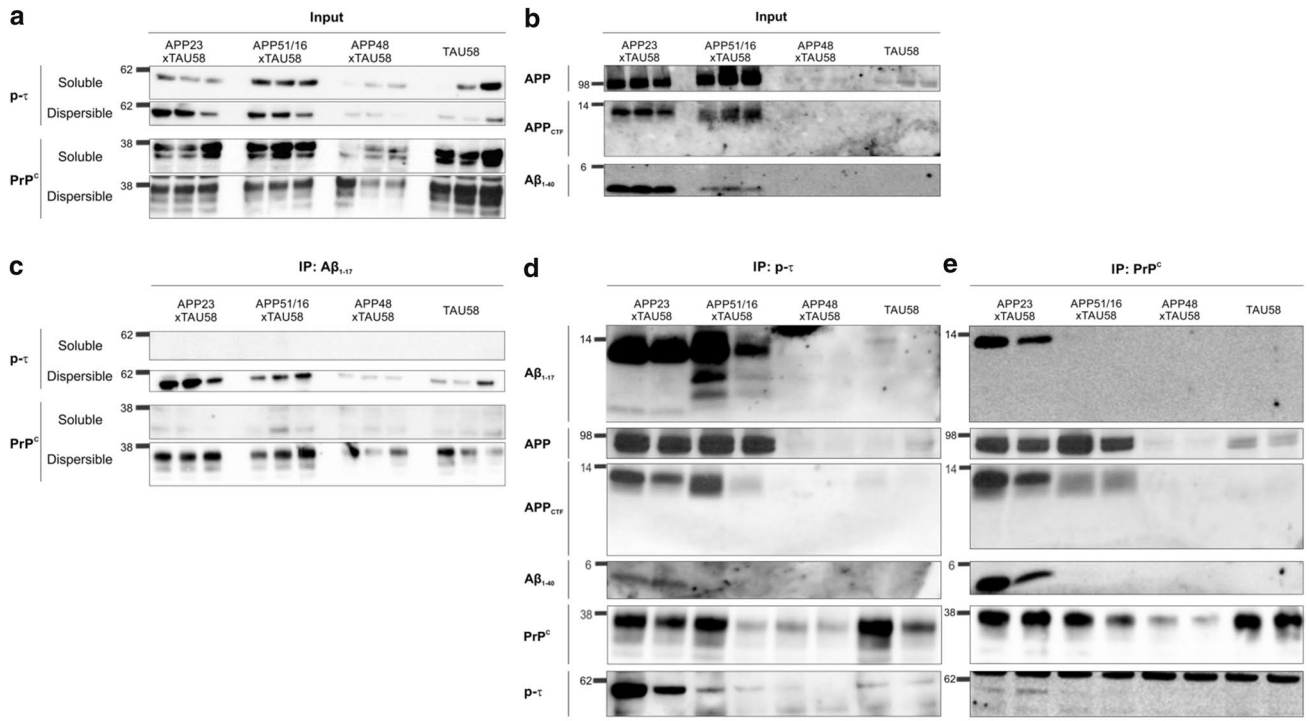

Fig. 3 Co-immunoprecipitation of Aβ, PrP^C and p-τ in APP23xTAU58, APP51/16xTAU58, APP48xTAU58, and TAU58 mice. **a** Input levels of PrP^C and p-τ in soluble and dispersible fractions of APP23xTAU58, APP51/16xTAU58, APP48xTAU58, and TAU58 mice determined by western blot analysis. **b** Input levels of APP, APP_{CTF}, and $Aβ_{40}$ in the dispersible fraction of the transgenic mice. $Aβ_{1–17}$ input is displayed in Fig. 2b. **c** Immunoprecipitation with anti-$Aβ_{1–17}$ antibodies (6E10) and subsequent western blot analysis of mouse forebrain homogenates with PrP^C (6D11) and p-τ (PHF-1) antibodies ($n = 5$). Both p-τ and PrP^C co-immunoprecipitated with Aβ in the dispersible fraction of APP23xTAU58 and APP51/16xTAU58 mice and less pronounced in APP48xTAU58 and TAU58 mice. There was no co-immunoprecipitation of p-τ and PrP^C in the soluble fraction. **d** In the dispersible fraction, $Aβ_{40}$, APP, APP_{CTF}, and PrP^C were detected by western blot analysis after immunoprecipitation with anti-p-τ antibodies in APP23xTAU58. In APP51/16xTAU58 mice, APP, APP_{CTF}, and PrP^C were also co-immunoprecipitated with p-τ. Co-immunoprecipitation of PrP^C was also seen in TAU58 mice. As positive control, the detection with anti-p-τ (AT8) confirmed immunoprecipitation of p-τ (**c**). **e** In the dispersible fraction of APP23xTAU58 mice, $Aβ_{40}$, APP, APP_{CTF}, and p-τ were detected by western blotting after immunoprecipitation with PrP^C. APP and APP_{CTF} were also found to be co-immunoprecipitated with PrP^C in APP51/16xTAU58 mice. As positive control, detection with anti-PrP^C (6D11) was used. **d**, **e** $Aβ_{1–17}$ and PrP^C or p-τ, $Aβ_{40}$, and APP_{CTF} were detected in the same membrane after stripping, respectively. Uncropped blots are provided in Suppl. Fig. 7

the dentate gyrus (Fig. 4s) in APP23xTAU58 (Fig. 4a–d, r–s) and APP51/16xTAU58 mice (Fig. 4e–h, r–s). Only single neurons in APP48xTAU58 mice were positive for all three proteins, $Aβ_{42}$, p-τ, and PrP^C (Fig. 4i–l, Table 2k), whereas TAU58 mice showed no Aβ-positive neurons. APP48xTAU58 and TAU58 mice exhibited lower numbers of PrP^C + p-τ double positive neurons than APP23xTAU58 and APP51/16xTAU58 mice, especially in the CA1 region (Fig. 4i–s, Table 2j, k). When analyzing PrP^C + p-τ double positive neurons for subcellular PrP^C–p-τ co-localization, the Pearson correlation coefficient was 0.35 (range: 0.035 to 0.85; Image J co-localization finder). No significant differences were observed among different mouse models or among different brain regions (frontal cortex, CA1, and dentate gyrus).

$Aβ_{42}$ was not detectable in APP23xTAU58 and APP51/16xTAU58 mice. Plaques were absent, also in the second set of triple label stainings using anti-p-τ (AT8), anti-$Aβ_{40}$ (polyclonal, IBL) or anti-$Aβ_{42}$ (polyclonal, IBL), and anti-PrP^C (6D11). Here, we could confirm co-localization of p-τ and PrP^C in neuronal perikarya of APP23xTAU58 and APP51/16xTAU58 mice (Suppl. Figure 9a–h). Single $Aβ_{40}$-positive dots were found in the neuropil of APP23xTAU58 mice co-localizing with PrP^C-positive material but not with p-τ (Suppl. Figure 9a–d). Single PrP^C and p-τ positive dot-like structures were also found in the neuropil of APP23xTAU58 and APP51/16xTAU58 mice (Suppl. Figure 9a–h). These dot-like structures were not abundant in APP48xTAU58 and TAU58 mice (Suppl. Figure 9i–p).

Proximity ligation assays (PLA) demonstrated close proximity (less than 30–40 nm distance) of PrP^C and p-τ in the cortex of all four different mouse lines, mainly in the neuropil (Fig. 5a, d, g, j). Proximity between PrP^C

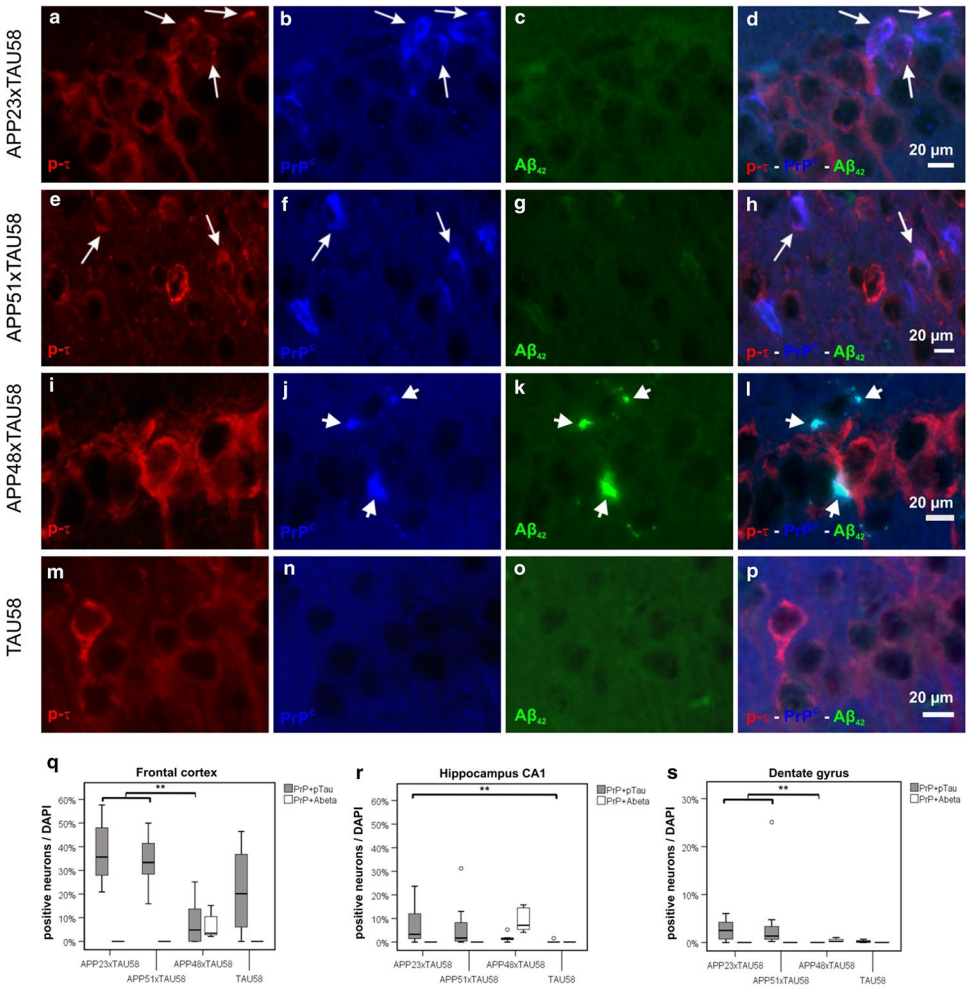

Fig. 4 Triple-label immunofluorescence of PrP^C, p-τ and Aβ in APP23xTAU58, APP51/16xTAU58, APP48xTAU58, and TAU58 mice. **a–p** Representative images of the triple-label immunofluorescence with antibodies raised against p-τ (1H6L6), PrP^C (6D11), and $Aβ_{42/43}$ (13D6) of the CA1/subiculum region of APP23xTAU58 (**a–d**), APP51/16xTAU58 (**e–h**), APP48xTAU58 (**i–l**), and TAU58 (**m–p**) mice. p-τ was detected with the 1H6L6 antibody and labelled in red with Cy5-linked secondary antibodies. PrP^C was detected with the 6D11 antibody labelled with Cy3-linked secondary antibodies and pseudo-coded in blue. Aβ was detected with the $Aβ_{42/43}$-specific antibody 13D6 and visualized in green by labelling with Cy2-linked secondary antibodies. Long arrows point to PrP^C + p-τ co-localization, whereas short arrows point to PrP^C + Aβ co-localization. PrP^C + p-τ double positive neurons as well as neurons exhibiting only PrP^C or p-τ were found in all four mouse lines, whereas co-localization of PrP^C and or p-τ with $Aβ_{42/43}$ was only found in APP48xTAU58 mice. **q–s** Quantification of PrP^C + p-τ double positive neurons and PrP^C + $Aβ_{42/43}$ double positive neurons in frontocentral cortex (**q**), CA1/subiculum (**r**), and dentate gyrus (**s**) of all transgenic lines. APP23xTAU58 and APP51/16xTAU58 mice displayed significantly higher percentages of PrP^C + p-τ double positive neurons compared to APP48xTAU58 in the frontocentral cortex and in the dentate gyrus. Compared to TAU58 mice, there was a trend for increased percentage of PrP^C + p-τ double positive neurons in the dentate gyrus of APP23xTAU58 and APP51/16xTAU58, albeit not significant. In the CA1/subiculum region, the APP23xTAU58 mice showed significantly higher percentage of PrP^C + p-τ double positive neurons than TAU58 mice. Similarly, in APP51/16xTAU58, a trend for increased percentage of PrP^C + p-τ double positive neurons in CA1 was observed. PrP^C + $Aβ_{42/43}$ double positive neurons were only detected in APP48xTAU58. Kruskal–Wallis H test corrected for multiple testing by the Bonferroni method: $*p<0.05$, $**p<0.01$; for detailed statistical analysis, see Table 2j, k. Number of mice: APP23xTAU58 mice: $n=6$; APP51/16xTAU58 mice: $n=7$; APP48xTAU58 mice: $n=5$; TAU58 mice: $n=8$. PrP^C and p-τ partially co-localized at the subcellular level, with an average of 0.35 Pearson's correlation coefficient (ranging from 0.035 to 0.85) as observed by analysis of PrP^C + p-τ double positive neurons among all mouse lines. No significant differences were seen between different mouse models or different brain regions (cortex, CA1 and dentate gyrus were assessed). Numbers of neurons assessed: APP23xTAU58 mice: $n=23$; APP51/16xTAU58 mice: $n=20$; APP48xTAU58 mice: $n=9$; TAU58 mice: $n=21$

and $Aβ_{40}$ was less prominent and restricted to few positive dots in APP23xTAU58 mice (Fig. 5a), as expected by the lack of Aβ-plaque pathology in these mice at 6 months of age (Suppl. Figure 8a–h). In APP51/16xTAU58, APP48xTAU58, and TAU58 mice, proximity between $Aβ_{40}$ and PrP^C was virtually absent. Only single dots were seen,

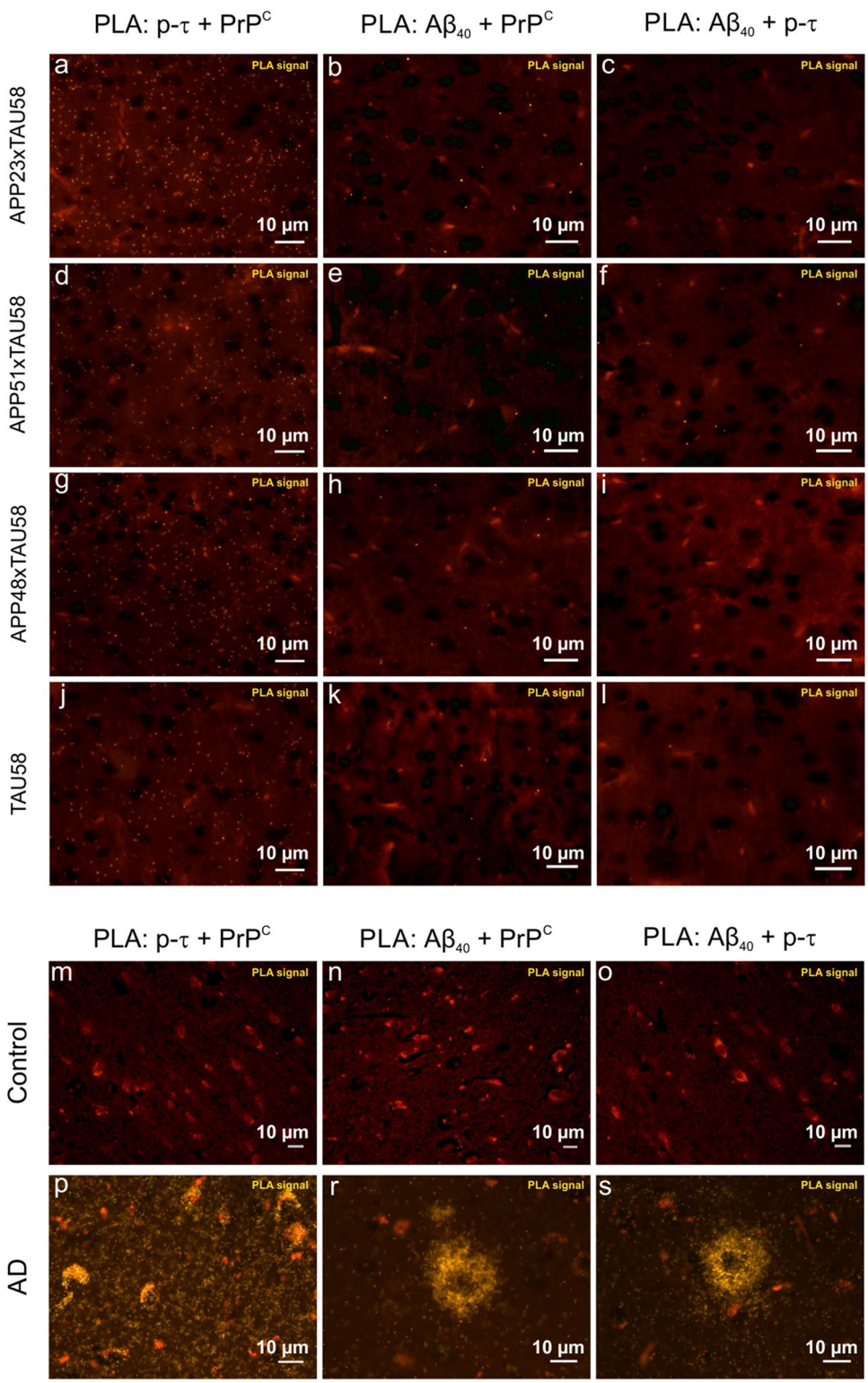

Fig. 5 Proximity ligation assays between PrP^C, p-τ, and $A\beta_{40}$ in transgenic mice and in human brain. **a**, **b** Representative images of three different proximity ligation assays (PLA): (1) p-τ/PrP^C (**a**, **d**, **g**, **j**, **m**, **p**); (2) $A\beta_{40}$/PrP^C (**b**, **e**, **h**, **k**, **n, r**); (3) $A\beta_{40}$/p-τ (**e**, **f**, **i**, **l**, **o**, **s**). Primary antibodies against p-τ (AT8 and 1H6L6), $A\beta_{40}$, and PrP^C (6D11) were used. **a**, **d**, **g**, **j** In all the transgenic mouse lines, p-τ and PrP^C were found in close proximity as seen by the dot-like PLA signal displayed in yellow–orange. **b**, **e**, **h**, **k** $A\beta_{40}$ and PrP^C proximity signal was restricted to few positive dots mainly detectable in APP23xTAU58 mice. **c**, **f**, **i**, **l** $A\beta_{40}$ and p-τ proximity was mostly absent, with a sparse-negligible signal in the APP51/16xTAU58 mice. **m–s** In the human brain, all combinations were positive in the AD case no. 8 (**p–s**) in comparison with the non-AD control case no. 17 (**m–o**), which had no PLA signal. Remarkably, p-τ and PrP^C proximity occurs both in few neuronal somata (co-localization of the PLA signal with neuronal lipofuscin autofluoresence) and in the neuropil (disperse signal) (**p**). On the other hand, the $A\beta_{40}$/PrP^C and the $A\beta_{40}$/p-τ PLA signal is observed in plaque-like structures and (less dense compared to plaques) in the neuropil

reflecting the unspecific signal of the assay (Fig. 5b, e, h, k). Proximity between $A\beta_{42}$ and PrP^C was most abundant in APP48xTAU58, as expected by its exclusive production of intracellular $A\beta_{42}$ (Suppl. Figure 10a–d), and in APP23xTAU58 mice. Aβ and p-τ proximity was virtually absent, with negligible residual signals in APP51/16xTAU58 mice (Fig. 5c, f, i, l). These results from single mice indicate that our immunohistochemical findings demonstrating co-localization of PrP^C and Aβ in APP23xTAU58 mice as well as of PrP^C and p-τ can, in all four mouse lines,

reflect proximity of the respective proteins, especially in the neuropil. The specificity of the PLA was confirmed in a human brain tissue section with antibodies against smooth muscle actin and tropomyosin that are specifically found in smooth muscle cells of blood vessels but not in the brain parenchyma (Suppl. Figure 10e, f). The PLA signal was found in blood vessels but not in the brain parenchyma. Here, only single dots indicated minimal random proximity in this negative control area.

PrP^C is associated with Aβ and p-τ in Alzheimer's disease

To confirm whether PrP^C association with Aβ and p-τ in mice showing accelerated spreading of p-τ pathology has relevance for human AD, we analyzed entorhinal cortex brain homogenates from postmortem brains of ten human AD, four control cases without Aβ pathology, and five non-demented cases with AD pathology considered to represent pathologically defined preclinical AD (p-preAD) cases [74] (Table 1). Biochemically, Aβ was observed in all AD and p-preAD cases, whereas sarkosyl-insoluble p-τ was present in all AD cases, p-preAD cases nos. 14 and 15, and non-AD case no. 16, which showed PART (Fig. 6a). Co-immunoprecipitation of sarkosyl-insoluble Aβ and p-τ with PrP^C was observed in 6 (Aβ) and 7 (p-τ) out of 10 AD cases but not in controls or p-preAD cases (Fig. 6b). Immunohistochemical analysis of sections from the medial temporal lobe revealed PrP^C in plaques in the temporal neocortex of 2 out of 9 AD and 3 out of 5 p-preAD cases. In two AD cases, cortical neurons were strongly PrP^C-positive, whereas a weak-to-moderate neuronal staining was observed in the remaining cases (Fig. 6c–h, Suppl. Figure 12, Table 1). In cases with this PrP^C pathology, the PrP^C in the lesions was digestible by proteinase K (Fig. 6f, g). Quantification of the percentage of temporal neocortex (area 36) neurons positive for PrP^C showed a trend towards a reduction in the AD group (Fig. 6i, Table 2l, m). Linear regression analysis revealed that the Aβ phases of the patients were associated with a mild decrease in the percentage of PrP^C-positive temporal neocortex neurons even when controlled for age and sex, whereas other AD-related parameters were not (Table 2l, m). Although 3 p-preAD and 2 AD cases exhibited PrP^C-positive plaques, linear regression analysis did not reveal a significant increase of the PrP^C-plaque load with increasing diagnosis stage (non-AD, p-preAD, and AD), CDR score, Aβ phase, Aβ plaque load, Braak-NFT stage, CERAD score for neuritic plaque pathology, and NIA-AA degree of AD pathology, whereas the Aβ load was associated with these parameters except for the CDR score even when controlled for age and sex (Table 2n, o). Aβ plaque loads were higher than PrP^C-plaque loads (Sign test: $p < 0.001$).

Proximity ligation assays showed that PrP^C and p-τ were in close proximity in AD (case no. 8) as opposed to a non-AD control case (case no. 17) (Fig. 5m–s). The proximity signal was found scattered throughout the neuropil and in single neurons resembling NFT-like structures (Fig. 5m, p). PrP^C and Aβ proximity was also found in this AD case in a scattered pattern in the neuropil (Fig. 5n, r). However, most signal clusters exhibited a plaque-like morphology. Likewise, Aβ and p-τ proximity occurred mostly in these structures, presumably reflecting the appearance of neuritic plaques (Fig. 5o, s). The scattered neuropil staining was not observed when a proximity ligation assay between smooth muscle actin and tropomyosin was performed for positive and negative control of the assay (Suppl. Figure 10e, f). In this case, the signal was specifically seen in smooth muscle cells of blood vessels, as expected. The brain parenchyma used as intrinsic negative control did not show proximity labeling except for very few dots in the neuropil indicative of negligible amounts of random proximity. These proximity patterns between PrP^C, p-τ, and Aβ were consistent with our immunohistochemical findings showing co-localization of Aβ and PrP^C in amyloid plaques and of p-τ and PrP^C in NFTs (Suppl. Figure 12). The increased proximity signal in the neuropil of AD cases reflected the expression of PrP^C in the neuropil and its proximity to p-τ-positive neuropil threads and to the soluble/dispersible Aβ in the neuropil, which initiates local plaque formation. The latter may become visible in proximity with PrP^C, because the proximity ligation assay uses rolling-circle amplification technology to amplify the signal in a manner that it can be detected, although it may not be seen by regular immunohistochemistry,

In vitro interaction of PrP^C with p-τ and Aβ

Pull-down experiments using recombinant his-tagged PrP^C to test binding to synthetic $A\beta_{40}$ and $A\beta_{42}$ demonstrated that PrP^C was able to interact directly with synthetic $A\beta_{40}$ and $A\beta_{42}$ in vitro, particularly to its dimeric forms as indicated by the presence of an 8 kDa band (Fig. 7). In the absence of PrP^C bait, $A\beta_{40}$ and $A\beta_{42}$ were unspecifically bound to the beads and detected in lower amounts than in the presence of his-tagged PrP^C. Especially, the 8 kDa band was virtually not seen in the absence of PrP^C bait. Moreover, his-PrP^C was also able to pull-down p-τ derived from a human AD brain homogenate. Aβ derived from the human AD brain homogenate was not pulled down by his-PrP^C in detectable amounts. For the interpretation of this finding, it should be mentioned that the Aβ concentration of the brain homogenate input was considerably lower than the concentration of the synthetic Aβ samples. Furthermore, the homogenates contained p-τ, which probably competed for binding to PrP^C. Accordingly, this assay demonstrated that $A\beta_{40}$, $A\beta_{42}$, and p-τ were able to

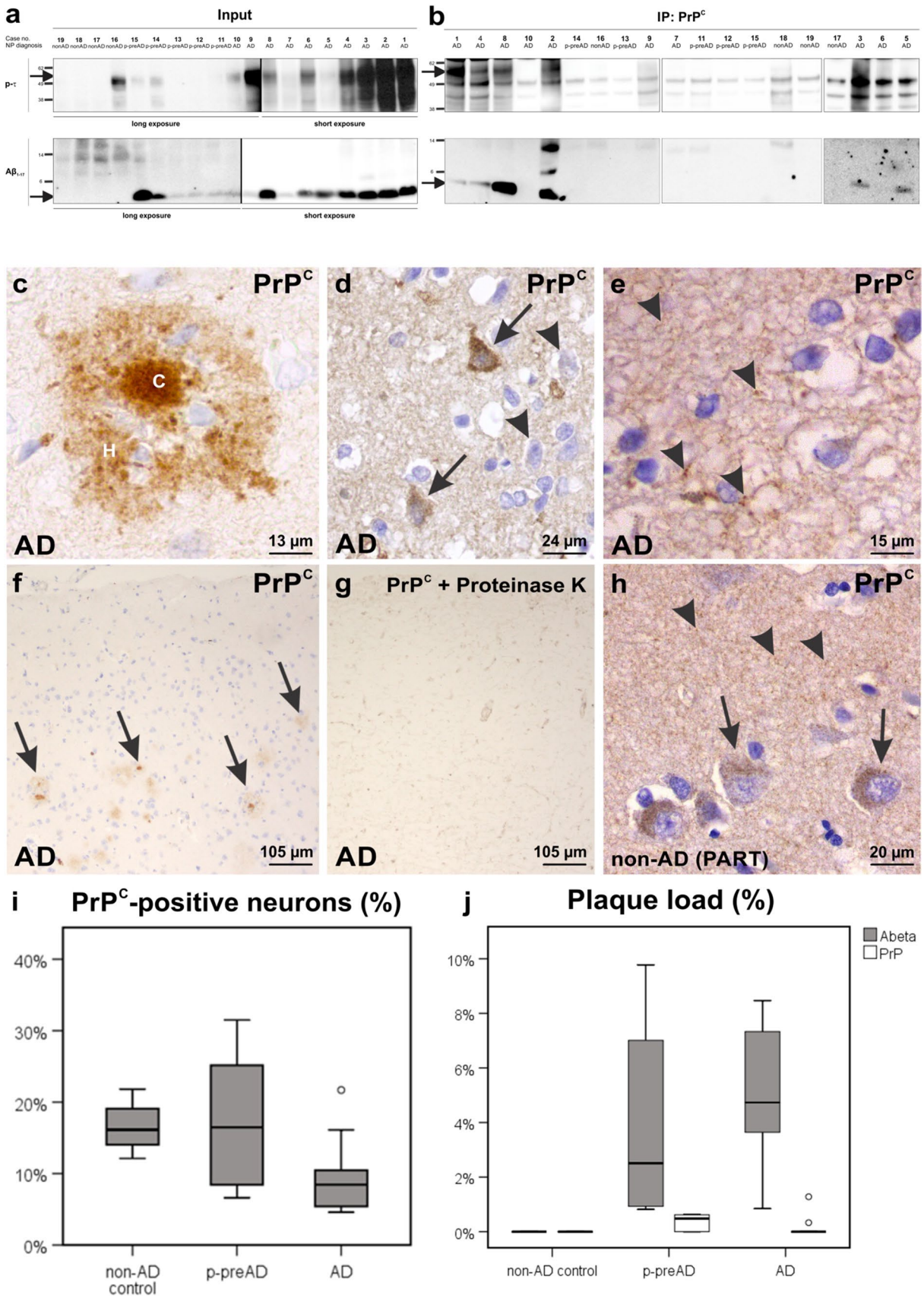
a
Input
b
IP: PrP^C
Case no.
NP diagnosis
p-τ
long exposure
short exposure
Aβ1-17
c
PrP^C
C
H
AD
13 µm
d
PrP^C
AD
24 µm
e
PrP^C
AD
15 µm
f
PrP^C
AD
105 µm
g
PrP^C + Proteinase K
AD
105 µm
h
PrP^C
non-AD (PART)
20 µm
i
PrP^C-positive neurons (%)
40%
30%
20%
10%
0%
non-AD control
p-preAD
AD
j
Plaque load (%)
Abeta
PrP
10%
8%
6%
4%
2%
0%
non-AD control
p-preAD
AD

◂**Fig. 6** Association of PrP^C with p-τ and Aβ in human Alzheimer's disease brain tissue. **a** Input levels of $Aβ_{1–17}$ and p-τ in the sarkosyl-insoluble fraction (P2) of entorhinal cortex brain homogenates from non-AD ($n=4$, including two PART cases), p-preAD ($n=5$), and sympAD ($n=10$) cases. $Aβ_{1–17}$ was detected after stripping the membranes stained with the PHF-1 antibody against p-τ. To document low levels in p-preAD, we showed longer exposures of the blots for these cases, whereas for AD cases, a shorter exposure time was already sufficient. Both short and long exposures of the entire blot are shown in Suppl. Figure 11. All AD cases showed high levels of Aβ and p-τ. The p-preAD cases showed low levels of Aβ. In two p-preAD cases and one non-AD case with PART (case no. 18), mildly increased levels of p-τ were observed. The respective bands for p-τ and Aβ were indicated by arrows. **b** Immunoprecipitation with the 6D11 antibody against PrP^C and subsequent western blot analysis with antibodies raised against p-τ (PHF-1) or $Aβ_{1–17}$ (6E10). Aβ was detected in 6 out of 10 AD cases and p-τ in 7 out of 10 AD cases, whereas no co-immunoprecipitation of PrP^C with p-τ or Aβ was observed in p-preAD and non-AD control cases. $Aβ_{1–17}$ was detected after stripping the membranes stained with the PHF-1 antibody against p-τ. The respective bands for p-τ and Aβ were indicated by arrows. **c–e** Presence of PrP^C in senile plaques (**c**; *C* amyloid core, *H* halo of diffuse Aβ) and neurons (arrows in **d**) in the temporal cortex (Brodmann are 36) of AD case no. 9 detected with the 3F4 anti-PrP^C antibody. In addition, AD cases showed a mild staining of the neuropil with few more strongly stained thread- and dot-like structures (arrowheads in **e**). Not all neurons exhibited PrP^C (arrowheads in **d**). **f** PrP^C in plaques was mainly restricted to layer III and deeper as demonstrated in case no. 8 (arrows in **f**; here stained with the 6D11 anti-PrP^C antibody). **f**, **g** The PrP^C deposits in AD-related changes (here stained with the 6D11 anti-PrP^C antibody) were digestible by proteinase K (**g**). **g** serves, thereby, also as a negative control for the anti-PrP^C antibody staining. **h** The neuropil staining (arrowheads) and the neuronal PrP^C staining (arrows) were also observed in non-AD controls (case no. 16). **i** Determination of the percentage of PrP^C-positive neurons in AD, p-preAD and non-AD control cases revealed a slightly lower percentage of PrP^C-positive neurons in AD cases than in non-AD controls and p-preAD cases which was not significant in linear regression models (Table 2l). **j** Likewise, the PrP^C-plaque load showed no significant differences among non-AD, p-preAD and AD cases, while there was a significant increase of the Aβ-plaque load in respective linear regression models (Table 2m). The Aβ-plaque loads were higher than the PrP^C-plaque loads (Sign test: $p<0.001$). Uncropped blots with molecular weight standards are provided in Suppl. Fig. 11. *NP diagnosis* = neuropathological diagnosis

interact directly with PrP^C in an in vitro system, when added in sufficient amounts.

Discussion

The main findings of this study are that: (1) extracellular soluble Aβ (in the absence of Aβ plaque pathology) was associated with spreading of p-τ pathology into further brain regions in APP23xTAU58 mice; (2) PrP^C was associated with this process; (3) human brain samples showed a similar association of PrP^C with Aβ and p-τ in 6 out of 10 AD cases; and (4) a pull-down assay confirmed the interaction of PrP^C with Aβ and p-τ.

The identification of spreading of p-τ pathology into the CA1 region of APP23xTAU58 and APP51/16xTAU58 mice was based on our finding that all of these animals showed p-τ pathology in the CA1 regions, whereas TAU58 and APP48xTAU58 mice showed no CA1 p-τ pathology in more than 50% of the animals. Accordingly, this region becomes affected around the age of 6 months in these animals and is more frequently affected in mice that have higher levels of soluble Aβ (APP23xTAU58) than in those without (TAU58 and APP48xTAU58). APP51/16xTAU58 mice had also detectable levels of soluble Aβ but quantitative analysis did not reveal a significant increase compared to TAU58 and APP48xTAU58 mice. Van Eersel et al. [95] described, in few TAU58 mice, Gallyas-positive neurons in CA1 already at 3 months of age. Therefore, one could argue that there is no spreading in TAU58 mice, because they already show NFTs in CA1 at 3 months of age. However, Van Eersel et al. [95] also described the lack of NFTs in the majority of the mice at this age. This is in line with our finding that more than 50% of 6-month-old TAU58 mice did not show CA1 p-τ pathology. Therefore, the presence of CA1-p-τ pathology in 100% of the APP23xTAU58 and APP51/16xTAU58 mice argues in favor of an involvement of a previously not-affected brain region (i.e., spreading of p-τ pathology in at least 50% of the animals). To what extent, this spreading means transneuronal propagation of seeds from one brain region to the next [19, 49] or just reflects pathology expansion into previously unaffected regions possibly also triggered by other factors, such as genetic factors, [81] remains open. The latter hypothesis is strongly supported by the fact that we compared different types of transgenic mice with different genetic backgrounds with impact on Aβ pathology. Due to the different genetic background, detectable amounts of soluble Aβ in APP23xTAU58 were associated with the consistent appearance of p-τ pathology in CA1, suggesting that this form of Aβ pathology can accelerate the propagation of p-τ pathology. This finding is supported by a trend towards increased levels of soluble Aβ in APP51/16xTAU58 mice, which also showed an accelerated spreading of p-τ pathology. Thus, a possible effect of soluble Aβ on p-τ-spreading may be related to its APP-derived production as seen in APP23xTAU58 and APP51/16xTAU58 mice resulting in its presence in the extracellular space [36]. Other forms of Aβ, such as dispersible, membrane-associated and formic acid-soluble Aβ, seem to be less important, because APP48xTAU58 mice exhibited these forms of Aβ, but did not show accelerated spreading (Fig. 8). Since the APP48 mice mainly produce intracellular Aβ [1], the extracellular presence of Aβ may be of importance for accelerating p-τ pathology.

Moreover, it had already been shown by others that τ-seeds derived from AD brain homogenates show stronger

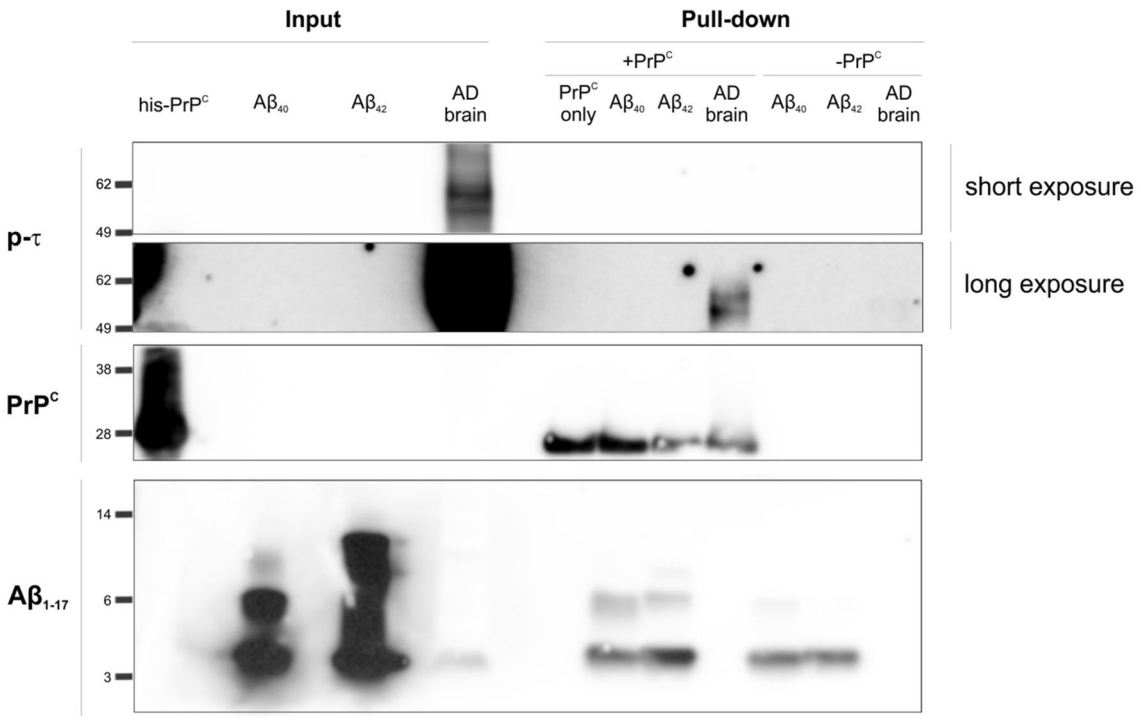

Fig. 7 Pull down of synthetic $A\beta_{40}$, $A\beta_{42}$, and p-τ derived from AD brain using recombinant PrP^C. Recombinant his-tagged PrP^C was used as a bait for testing the interaction with synthetic $A\beta_{40}$, synthetic $A\beta_{42}$, and p-τ derived from AD brain. When the amount of $A\beta_{40}$ and $A\beta_{42}$ in the presence or absence of his-PrP^C were compared, increased amounts of $A\beta_{40}$ and $A\beta_{42}$ were observed when incubated with his-PrP^C. The Aβ signal observed in the absence of his-PrP^C was attributed to unspecific binding of Aβ to the nickel-resin beads. Notably, the dimeric Aβ bands (~8 kDA) seem to be more effectively pulled down than monomeric Aβ. Aβ derived from human brain was not pulled down, which may be due to the relatively small amount of Aβ in the brain extract (see input) when compared to the amount of synthetic Aβ used (5 µg). Moreover, his-PrP^C was able to bind p-τ from the brain extract as indicated by increased p-τ levels when incubated with his-PrP^C. A long exposure image is depicted for better visualization. Antibodies raised against p-τ (PHF1), PrP^C (6D11), and $A\beta_{1-17}$ (6E10) were used for western blot detection

seeding effects in the presence of Aβ plaque pathology [99] and can form the entire spectrum of AD lesions including neuritic plaques in the presence of Aβ pathology but not in its absence [38]. Our findings of an accelerated spreading of p-τ into the hippocampus in the presence of increased levels of soluble Aβ would fit into the context of these and earlier studies pointing to an acceleration of p-τ pathology by Aβ [30, 54].

PrP^C was associated with both Aβ and p-τ in the dispersible fraction of brain homogenates from APP23xTAU58 and APP51/16xTAU58 mice. In a mouse model that produces exclusively intracellular $A\beta_{42}$ aggregates independent from APP, the APP48xTAU58 mouse, p-τ pathology was not increased and co-immunoprecipitation with Aβ or p-τ showed similar or lower levels of PrP^C compared to TAU58 mice. Co-immunoprecipitation of PrP^C also revealed that APP and C-terminal fragments of APP, such as $APP_{CTF\alpha}$ and $APP_{CTF\beta}$, interact with PrP^C suggesting a role for PrP^C in the interaction of APP/Aβ with p-τ. In the human brain, co-immunoprecipitation of PrP^C with dispersible p-τ in 7 out of 10 AD cases and with dispersible Aβ in 6 out of 10 AD cases indicated that PrP^C may also play a role in AD pathogenesis. Here, a specific interaction with APP or its C-terminal fragments was not observed. A direct interaction of PrP^C with p-τ and Aβ could be confirmed in vitro with a pull-down assay, and by demonstrating proximity of less than 30–40 nm of Aβ and PrP^C as well as of p-τ and PrP^C in an AD case and in transgenic mouse brain. These observations confirm previous studies showing the interaction of Aβ oligomers and PrP^C in vitro [5] and in vivo [24, 29]. Although PrP^C has been seen co-localizing with NFTs and interacting with p-τ in Gerstmann–Sträussler–Scheinker syndrome [46, 103], the interaction of PrP^C with p-τ and its association with p-τ propagation is novel, may explain the modulation of changes in long-term potentiation/depression after treatment with soluble τ aggregates by PrP^C [66, 67], and supports the hypothesis that PrP^C plays a role in the pathogenesis of AD [105]. Such a role of PrP^C in AD would be in line with the finding of others that deletion of PrP^C results in a rescue of APPswe/PS1DeltaE9 mice from behavioral deficits and synapse loss [29, 78] and that the absence of PrP^C in PrP^C-knockout mice reduced Aβ

pathology [68]. The mechanism proposed for PrP^C is that of an interaction partner of soluble Aβ oligomers activating Fyn [22, 78, 94], which itself increases the levels of p-τ via Pyk2-related phosphorylation of τ [18, 20, 56] (Fig. 8). Experiments based on Aβ oligomer-treated primary neuronal cell cultures showed that PrP^C downregulated τ expression and phosphorylation in the presence of Aβ oligomers when compared to PrP^C-knockout cells, and, therefore, might protect against the development of AD p-τ pathology [100]. On the other hand, other authors found no such protective effect of PrP^C when treating wild-type and PrP^C-knockout mice with Aβ oligomers, or when crossing APP/PS1 mice with PrP^C-knockout or -overexpressing mice and assessing its memory function [5, 17]. Together with our findings, it is tempting to speculate that the interaction of soluble Aβ oligomers with PrP^C, resulting in dispersible Aβ–PrP^C complexes, may limit the capacity of PrP^C to further protect from τ phosphorylation/accumulation, probably by competition between soluble Aβ and soluble p-τ for binding to PrP^C. Soluble p-τ has been shown to be released at synapses [16] and is, in doing so, present in the extracellular space and can potentially bind to PrP^C. To what extent endosomal trafficking or lysosomal degradation of PrP^C and/or τ are involved in PrP^C–p-τ interactions needs to be clarified in the future. Our finding of a direct interaction between PrP^C and p-τ as well as between PrP^C and Aβ in the pull-down assay would argue in favor of such a potentially competitive interaction as hypothesized in Fig. 8. Alteration of the balance between PrP^C, Fyn activation, and τ-protein phosphorylation by binding of Aβ to PrP^C is an alternative explanation for accelerating τ phosphorylation via a PrP^C-related mechanism [51]. The finding that the Fyn inhibitor saracatinib improved memory function in APPswe/PS1DeltaE9 mice [31, 82] would support the latter hypothesis.

A possible limitation of our study is the fact that not all AD cases showed co-immunoprecipitation of PrP^C with Aβ and p-τ. Either this interaction does not represent a general mechanism of AD but a pathomechanism in a subgroup of AD patients, or postmortem degradation of proteins, fixation issues, or differences in protein expression during the agonal phase account for differences in the immunoprecipitation findings. Given the findings in mice, we would favor the second explanation, but cannot exclude that there are indeed different types of AD based on the contribution of PrP^C.

The β-site APP-cleaving enzyme 1 (BACE1) activity has been shown to be decreased in the presence of PrP^C [31, 70] and a regulation of PrP^C expression by a presenilin/APP intracellular domain (AICD)-related mechanism has been controversially discussed [55, 101]. Since APP-overexpressing APP23xTAU58 and APP51/16xTAU58 mice had high levels of PrP^C in the soluble and dispersible fraction, one could interpret this finding as a regulatory effect potentially linked to APP metabolism. However, TAU58 mice without APP overexpression did not differ in the level of PrP^C expression compared to APP23xTAU58 and APP51/16xTAU58 mice. Therefore, the increased levels of PrP^C seen in APP23xTAU58 and APP51/16xTAU58 mice are not necessarily linked to an effect of the APP metabolism, but may alternatively be related to τ expression, probably as compensatory effect on the transgenic overexpression of the τ protein in the mouse models used.

Moreover, PrP^C-positive plaques and neurons were described in AD cases [23, 26, 72, 98] as well as a reduction of the PrP^C content in the cortex and hippocampus of AD cases compared to controls [98, 106, 107]. However, other authors described increased numbers of PrP^C-positive neurons in AD cases compared to controls [102]. Given the high variance of the percentage of PrP^C-positive neurons in our small sample and inconsistent findings of other authors, more comprehensive histopathological studies on PrP^C in AD addressing the tissue and staining quality issues will be required in the future. The proximity of PrP^C and p-τ in few neurons of an AD case, the PrP^C-positivity of p-τ containing neurons in mice and AD cases, as well as the PrP^C expression of Aβ plaques in some AD and p-preAD cases supports the hypothesis that PrP^C can interact with Aβ and p-τ in an AD-specific manner. The cortical neuropil was the main site where proximity between PrP^C and Aβ and between PrP^C and p-τ occurred. This fits well with the known neuropil-staining pattern of PrP^C in the cortex [72] and may reflect the main site of pathological interaction of PrP^C with Aβ or p-τ, because Aβ plaques and p-τ containing neuropil threads develop in the neuropil as well. However, future ultrastructural analysis will be required because it is important to note that proximity ligation assay shows only proximity of two molecules regardless of whether they physically interact or show random proximity. That PrP^C can physically interact with Aβ and p-τ was shown here by the pull-down assay and co-immunoprecipitation experiments indicating PrP^C bound to Aβ and/or p-τ in APP23xTAU58 mouse brain and in 60% of the AD brains studied. That this co-immunoprecipitation effect was not only seen in AD cases with amyloid plaques but also in APP23xTAU58 mouse brain, strongly argues against an unspecific binding of PrP^C to plaque-amyloid, e.g., in dystrophic neurites of neuritic plaques, because 9 out of 10 APP23xTAU58 mice studied here exhibited no amyloid plaques.

Accordingly, the results of this study support a critical role of PrP^C in AD pathogenesis [93], particularly as a mediator for accelerating p-τ spreading (Fig. 8). Since APP-transgenic mice that do not overexpress τ-protein, do not develop significant p-τ pathology [28, 40, 85], and since the presence of the τ-protein in general has been shown to be a prerequisite for Aβ-induced neurotoxicity [76], a preexisting p-τ pathology appears to be a prerequisite for Aβ to aggravate p-τ pathology [30, 54]. The failure of PrP^C-knockout and

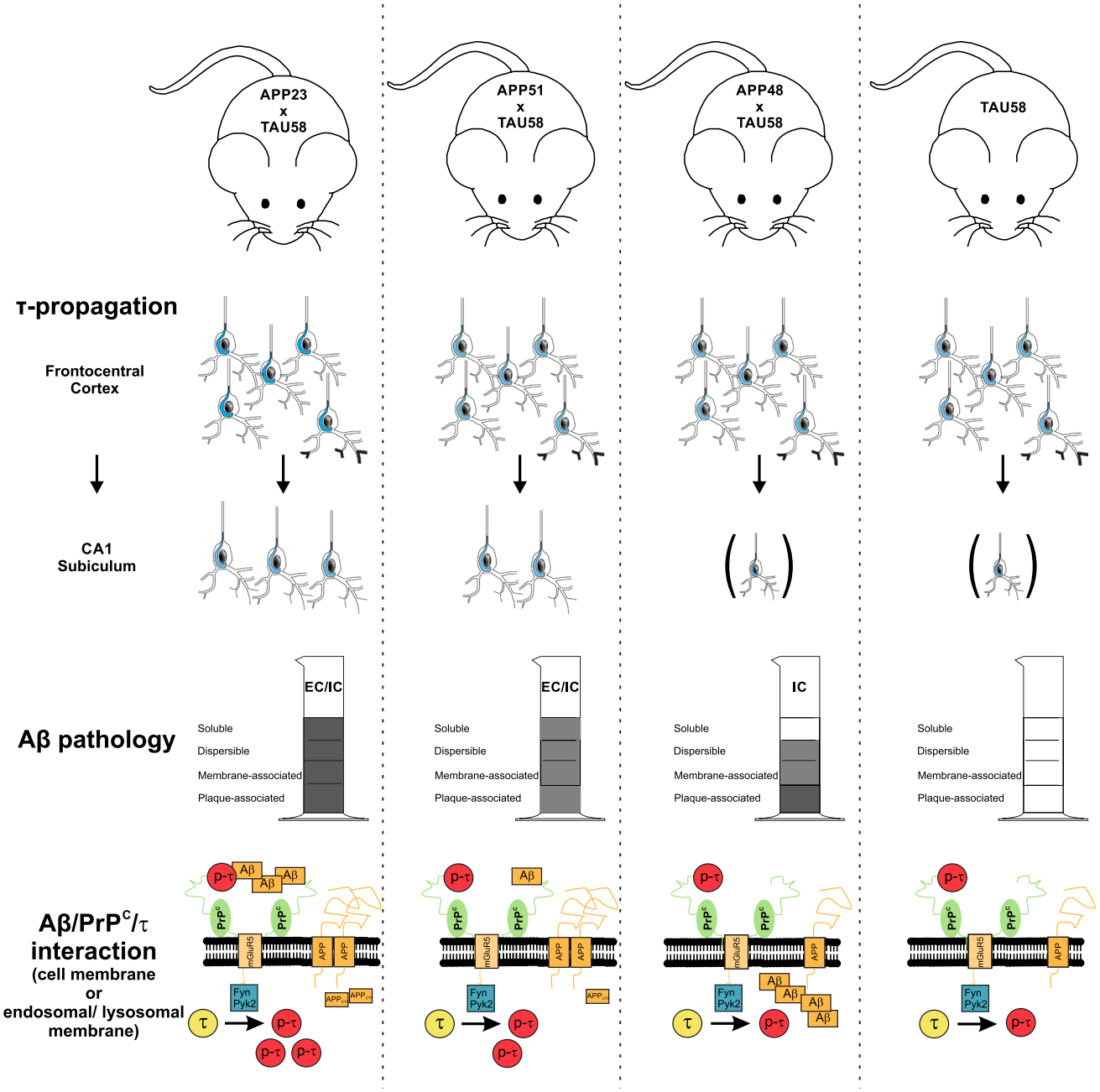

PrP^C-overexpressing mice to improve or modify cognition in APP/PS1-transgenic mice [5, 17] without additional overexpression of pathological τ-protein may support the role of a preexisting τ-pathology before the Aβ–PrP^C interaction receives pathogenic relevance. This concept of a preexisting tauopathy, which exacerbates in the presence of soluble Aβ leading to the typical pattern of AD pathology [84], is in line with data from autopsy studies [12]. It supports our hypothesis that the interaction of p-τ and PrP^C appears to be a prerequisite for Aβ to accelerate p-τ pathology.

In the light of novel PrP^C targeting treatment strategies, such as blocking Aβ binding to PrP^C or interfering with Fyn or Pyk2 functions, all leading to better cognitive performance of APP/PS1-transgenic mice [21, 35, 82], our results may have impact on the design of clinical studies with these compounds. First, we have seen that a large group of the AD cases, but not all, showed co-immunoprecipitation of PrP^C with Aβ and p-τ or the presence of PrP^C-positive plaques. This means that these cases showing PrP^C-related Aβ binding should be identified as a target group to test compounds targeting PrP^C to be sure to treat those patients that should theoretically profit. Moreover, our finding that PrP^C seems to be involved in the acceleration of p-τ pathology spreading indicated that biomarkers focusing on p-τ pathology,

◂**Fig. 8** Schematic summary. Transgenic mice producing APP-derived Aβ (APP23xTAU58 and APP51/16xTAU58) exhibit more widespread p-τ pathology than mice exclusively generating intracellular Aβ (APP48xTAU58) and single τ-transgenic mice (TAU58). Although all four transgenic mouse lines have p-τ pathology in the frontocentral cortex at 6 months of age, APP23xTAU58 and APP51/16xTAU58 show a significantly increased percentage of p-τ-positive neurons in the CA1 hippocampal area, which was affected in all animals, whereas less than 50% of the TAU58 and APP48xTAU58 mice showed p-τ lesions in this region. The APP23xTAU58 and APP51/16xTAU58 mice also display higher levels of soluble and dispersible Aβ, whereas APP48xTAU58 mice have the tendency to accumulate more insoluble Aβ aggregates (formic acid-soluble/plaque-associated material). Thus, propagation of p-τ pathology in APP23xTAU58 and APP51/16xTAU58 mice appears to be triggered by presumably extracellular soluble Aβ. Given the interaction of both Aβ and p-τ with PrP^C in vitro, in mice and in AD cases, it is tempting to hypothesize that extracellular Aβ and p-τ can interact with PrP^C. In the event that there is an accelerated propagation of p-τ, both p-τ and Aβ bind to PrP^C, whereas in the absence of extracellular Aβ, p-τ propagation was not accelerated. Even the presence of intracellular Aβ in APP48xTAU58 mice was not sufficient to accelerate p-τ propagation. Since APP23 mice without transgenic τ-protein expression do not show significant NFT pathology [85], it appears likely that binding of Aβ to PrP^C accelerates a process that has been started by the presence of p-τ also interacting with PrP^C. Based on the work of others [13, 51, 53, 56, 77], PrP^C-related mechanisms can cause activation of Fyn/Pyk2-related phosphorylation of τ through mGluR5 receptors, probably causing increased production of p-τ, which results in an accelerated spreading of p-τ pathology. Whether this mechanism leads to increased p-τ or whether PrP^C is involved in lysosomal p-τ clearance [15, 71], which may be impaired by Aβ interacting with the PrP^C–p-τ complexes, needs to be clarified in the future. *EC* Extracellular, *IC* Intracellular

such as cerebrospinal fluid p-τ or τ-PET [79, 96], should be used to document a potential effect of the above-mentioned compounds in clinical studies. Since the progression of p-τ pathology correlates well with increasing degree of dementia [3, 6, 89], effects of PrP^C-modifying compounds on p-τ pathology should also go along with a clinical improvement or at least stop of progression in cases susceptible for modifications of PrP^C function.

Together, our findings expand the knowledge about the role of PrP^C in Alzheimer's disease, particularly in the interplay between Aβ and τ. Preexisting p-τ pathology interacting with PrP^C, thereby, appears to be a prerequisite for Aβ to function as a p-τ pathology accelerator. Thus, PrP^C may act as an important mediator of Aβ-driven effects on p-τ pathology, which may provide a novel therapeutic target for stopping p-τ spreading and its downstream neurodegenerative and cognitive consequences in a large group of AD cases.

Acknowledgements We thank Dr. Peter Davies, Department of Pathology, Albert Einstein College of Medicine, USA for the gift of the PHF1 and TG3 antibodies and Dr. Marcus Fändrich, Institute of Pharmaceutical Biotechnology, Center for Biomedical Research, University of Ulm, Germany for the gift of B10AP antibody fragments. The administrative and technical help of Mrs. Alicja Ronisz is gratefully acknowledged.

Author contributions Study design: DRT and MS; biochemistry: SAH, LAG, ARU, PLB, VU, KB, RF, CG, and MW; histology: SAH, ARU, MJK, SO, LAG, and DRT; animal experiments: JR, SR, and MS; neuropathology: DRT and TT; clinical neurology: RV and CAFA. Statistical analysis: DRT, LAG, and SAH. Data interpretation: DRT, LAG, and SAH; manuscript preparation: SAH, LAG, and DRT; critical manuscript review: ARU, KB, MJK, SO, PLB, VU, JR, SR, RV, CAFA, TT, RF, CG, MW, and MS.

Funding Alzheimer Forschung Initiative (AFI) #10810 (DRT); Fonds Wetenschappelijk Onderzoek (FWO) G0F8516N (DRT, RV); Vlaamse Impulsfinanciering voor Netwerken voor Dementie-onderzoek (IWT 135043) (RV, DRT).

Compliance with ethical standards

Conflict of interest DRT received consultant honorary from GE-Healthcare (UK), and Covance Laboratories (UK), speaker honorary from Novartis Pharma AG (Switzerland), travel reimbursement from GE-Healthcare (UK), and UCB (Belgium), and collaborated with Novartis Pharma AG (Switzerland), Probiodrug (Germany), GE-Healthcare (UK), and Janssen Pharmaceutical Companies (Belgium). JR and MS were employees of Novartis Pharma Basel and SR is employee of Novartis Pharma Basel (Switzerland). CAFvA received honoraria from serving on the scientific advisory board of Nutricia GmbH (2014), Roche (2018) and Honkong University Research Council (2014) and has received funding for travel and speaker honoraria from Nutricia GmbH (2014–2015), Lilly Deutschland GmbH (2013–2016), Desitin Arzneimittel GmbH (2014), Biogen (2016–2018), Roche (2017–2018), and Dr. Willmar Schwabe GmbH&Co. KG (2014–2015).

References

1. Abramowski D, Rabe S, Rijal Upadhaya A, Reichwald J, Danner S, Staab D et al (2012) Transgenic expression of intraneuronal Abeta42 but not Abeta40 leads to cellular Abeta lesions, degeneration and functional impairment without typical Alzheimer's disease pathology. J Neurosci 32:1273–1283
2. Alzheimer A (1907) Ueber eine eigenartige Erkrankung der Hirnrinde. Allg Zschr Psych 64:146–148
3. Arriagada PV, Growdon JH, Hedley-Whyte ET, Hyman BT (1992) Neurofibrillary tangles but not senile plaques parallel duration and severity of Alzheimer's disease. Neurology 42:631–639
4. Attems J, Thomas A, Jellinger K (2012) Correlations between cortical and subcortical tau pathology. Neuropathol Appl Neurobiol 38:582–590
5. Balducci C, Beeg M, Stravalaci M, Bastone A, Sclip A, Biasini E et al (2010) Synthetic amyloid-beta oligomers impair long-term memory independently of cellular prion protein. Proc Natl Acad Sci USA 107:2295–2300
6. Bancher C, Braak H, Fischer P, Jellinger KA (1993) Neuropathological staging of Alzheimer lesions and intellectual status in Alzheimer's and Parkinson's disease patients. Neurosci Lett 162:179–182
7. Braak H, Alafuzoff I, Arzberger T, Kretzschmar H, Del Tredici K (2006) Staging of Alzheimer disease-associated neurofibrillary pathology using paraffin sections and immunocytochemistry. Acta Neuropathol 112:389–404

8. Braak H, Braak E (1991) Demonstration of amyloid deposits and neurofibrillary changes in whole brain sections. Brain Pathol 1:213–216
9. Braak H, Braak E (1991) Neuropathological stageing of Alzheimer-related changes. Acta Neuropathol 82:239–259
10. Braak H, Del Tredici K (2011) Alzheimer's pathogenesis: is there neuron-to-neuron propagation? Acta Neuropathol 121:589–595
11. Braak H, Del Tredici K (2011) The pathological process underlying Alzheimer's disease in individuals under thirty. Acta Neuropathol 121:171–181
12. Braak H, Thal DR, Ghebremedhin E, Del Tredici K (2011) Stages of the pathological process in Alzheimer's disease: age categories 1 year to 100 years. J Neuropathol Exp Neurol 70:960–969
13. Brody AH, Strittmatter SM (2018) Synaptotoxic signaling by amyloid beta oligomers in Alzheimer's disease through prion protein and mGluR5. Adv Pharmacol 82:293–323
14. Buee L, Bussiere T, Buee-Scherrer V, Delacourte A, Hof PR (2000) Tau protein isoforms, phosphorylation and role in neurodegenerative disorders. Brain Res Brain Res Rev 33:95–130
15. Caballero B, Wang Y, Diaz A, Tasset I, Juste YR, Stiller B et al (2018) Interplay of pathogenic forms of human tau with different autophagic pathways. Aging Cell 17:e12692
16. Calafate S, Buist A, Miskiewicz K, Vijayan V, Daneels G, de Strooper B et al (2015) Synaptic contacts enhance cell-to-cell tau pathology propagation. Cell Rep 11:1176–1183
17. Calella AM, Farinelli M, Nuvolone M, Mirante O, Moos R, Falsig J et al (2010) Prion protein and Abeta-related synaptic toxicity impairment. EMBO Mol Med 2:306–314
18. Chen RJ, Chang WW, Lin YC, Cheng PL, Chen YR (2013) Alzheimer's amyloid-beta oligomers rescue cellular prion protein induced tau reduction via the Fyn pathway. ACS Chem Neurosci 4:1287–1296
19. Clavaguera F, Bolmont T, Crowther RA, Abramowski D, Frank S, Probst A et al (2009) Transmission and spreading of tauopathy in transgenic mouse brain. Nat Cell Biol 11:909–913
20. Cline EN, Bicca MA, Viola KL, Klein WL (2018) The amyloid-beta oligomer hypothesis: beginning of the third decade. J Alzheimers Dis 64:S567–S610
21. Cox TO, Gunther EC, Brody AH, Chiasseu MT, Stoner A, Smith LM et al (2019) Anti-PrP(C) antibody rescues cognition and synapses in transgenic alzheimer mice. Ann Clin Transl Neurol 6:554–574
22. De Mario A, Castellani A, Peggion C, Massimino ML, Lim D, Hill AF et al (2015) The prion protein constitutively controls neuronal store-operated Ca(2+) entry through Fyn kinase. Front Cell Neurosci 9:416
23. Esiri MM, Carter J, Ironside JW (2000) Prion protein immunoreactivity in brain samples from an unselected autopsy population: findings in 200 consecutive cases. Neuropathol Appl Neurobiol 26:273–284
24. Falker C, Hartmann A, Guett I, Dohler F, Altmeppen H, Betzel C et al (2016) Exosomal cellular prion protein drives fibrillization of amyloid beta and counteracts amyloid beta-mediated neurotoxicity. J Neurochem 137:88–100
25. Ferreira DG, Temido-Ferreira M, Vicente Miranda H, Batalha VL, Coelho JE, Szego EM et al (2017) alpha-synuclein interacts with PrP(C) to induce cognitive impairment through mGluR5 and NMDAR2B. Nat Neurosci 20:1569–1579
26. Ferrer I, Blanco R, Carmona M, Puig B, Ribera R, Rey MJ et al (2001) Prion protein expression in senile plaques in Alzheimer's disease. Acta Neuropathol 101:49–56
27. Fredriksson S, Gullberg M, Jarvius J, Olsson C, Pietras K, Gustafsdottir SM et al (2002) Protein detection using proximity-dependent DNA ligation assays. Nat Biotechnol 20:473–477
28. Games D, Adams D, Alessandrini R, Barbour R, Berthelette P, Blackwell C et al (1995) Alzheimer-type neuropathology in transgenic mice overexpressing V717F beta-amyloid precursor protein. Nature 373:523–527
29. Gimbel DA, Nygaard HB, Coffey EE, Gunther EC, Lauren J, Gimbel ZA et al (2010) Memory impairment in transgenic Alzheimer mice requires cellular prion protein. J Neurosci 30:6367–6374
30. Gotz J, Chen F, van Dorpe J, Nitsch RM (2001) Formation of neurofibrillary tangles in P301l tau transgenic mice induced by Abeta 42 fibrils. Science 293:1491–1495
31. Griffiths HH, Whitehouse IJ, Hooper NM (2012) Regulation of amyloid-beta production by the prion protein. Prion 6:217–222
32. Grinberg LT, Rub U, Ferretti RE, Nitrini R, Farfel JM, Polichiso L et al (2009) The dorsal raphe nucleus shows phospho-tau neurofibrillary changes before the transentorhinal region in Alzheimer's disease. A precocious onset? Neuropathol Appl Neurobiol 35:406–416
33. Grundke-Iqbal I, Iqbal K, Quinlan M, Tung YC, Zaidi MS, Wisniewski HM (1986) Microtubule-associated protein tau. A component of Alzheimer paired helical filaments. J Biol Chem 261:6084–6089
34. Grundke-Iqbal I, Iqbal K, Tung YC, Quinlan M, Wisniewski HM, Binder LI (1986) Abnormal phosphorylation of the microtubule-associated protein tau (tau) in Alzheimer cytoskeletal pathology. Proc Natl Acad Sci USA 83:4913–4917
35. Gunther EC, Smith LM, Kostylev MA, Cox TO, Kaufman AC, Lee S et al (2019) Rescue of transgenic Alzheimer's pathophysiology by polymeric cellular prion protein antagonists. Cell Rep 26(145–158):e8
36. Haass C, Schlossmacher MG, Hung AY, Vigo-Pelfrey C, Mellon A, Ostaszewski BL et al (1992) Amyloid beta-peptide is produced by cultured cells during normal metabolism. Nature 359:322–325
37. Habicht G, Haupt C, Friedrich RP, Hortschansky P, Sachse C, Meinhardt J et al (2007) Directed selection of a conformational antibody domain that prevents mature amyloid fibril formation by stabilizing Abeta protofibrils. Proc Natl Acad Sci USA 104:19232–19237
38. He Z, Guo JL, McBride JD, Narasimhan S, Kim H, Changolkar L et al (2018) Amyloid-beta plaques enhance Alzheimer's brain tau-seeded pathologies by facilitating neuritic plaque tau aggregation. Nat Med 24:29–38
39. Herzig MC, Winkler DT, Burgermeister P, Pfeifer M, Kohler E, Schmidt SD et al (2004) Abeta is targeted to the vasculature in a mouse model of hereditary cerebral hemorrhage with amyloidosis. Nat Neurosci 7:954–960
40. Hsiao K, Chapman P, Nilsen S, Eckman C, Harigaya Y, Younkin S et al (1996) Correlative memory deficits, Abeta elevation, and amyloid plaques in transgenic mice. Science 274:99–102
41. Hsu SM, Raine L, Fanger H (1981) Use of avidin-biotin-peroxidase complex (ABC) in immunoperoxidase techniques: a comparison between ABC and unlabeled antibody (PAP) procedures. J Histochem Cytochem 29:577–580
42. Hu NW, Corbett GT, Moore S, Klyubin I, O'Malley TT, Walsh DM et al (2018) Extracellular forms of Abeta and tau from iPSC models of Alzheimer's disease disrupt synaptic plasticity. Cell Rep 23:1932–1938
43. Hughes CP, Berg L, Danziger WL, Coben LA, Martin RL (1982) A new clinical scale for the staging of dementia. Br J Psychiatry 140:566–572
44. Hurtado DE, Molina-Porcel L, Iba M, Aboagye AK, Paul SM, Trojanowski JQ et al (2010) A{beta} accelerates the spatiotemporal progression of tau pathology and augments tau amyloidosis in an Alzheimer mouse model. Am J Pathol 177:1977–1988

45. Hyman BT, Phelps CH, Beach TG, Bigio EH, Cairns NJ, Carrillo MC et al (2012) National institute on aging—Alzheimer's Association guidelines for the neuropathologic assessment of Alzheimer's disease. Alzheimers Dement 8:1–13
46. Ishizawa K, Komori T, Shimazu T, Yamamoto T, Kitamoto T, Shimazu K et al (2002) Hyperphosphorylated tau deposition parallels prion protein burden in a case of Gerstmann–Straussler–Scheinker syndrome P102L mutation complicated with dementia. Acta Neuropathol 104:342–350
47. Ittner LM, Ke YD, Delerue F, Bi M, Gladbach A, van Eersel J et al (2010) Dendritic function of tau mediates amyloid-beta toxicity in Alzheimer's disease mouse models. Cell 142:387–397
48. Jicha GA, Lane E, Vincent I, Otvos L Jr, Hoffmann R, Davies P (1997) A conformation- and phosphorylation-dependent antibody recognizing the paired helical filaments of Alzheimer's disease. J Neurochem 69:2087–2095
49. Jucker M, Walker LC (2011) Pathogenic protein seeding in Alzheimer disease and other neurodegenerative disorders. Ann Neurol 70:532–540
50. Kayed R, Head E, Thompson JL, McIntire TM, Milton SC, Cotman CW et al (2003) Common structure of soluble amyloid oligomers implies common mechanism of pathogenesis. Science 300:486–489
51. Larson M, Sherman MA, Amar F, Nuvolone M, Schneider JA, Bennett DA et al (2012) The complex PrP(c)–Fyn couples human oligomeric Abeta with pathological tau changes in Alzheimer's disease. J Neurosci 32:16857-71a
52. Lau DH, Hogseth M, Phillips EC, O'Neill MJ, Pooler AM, Noble W et al (2016) Critical residues involved in tau binding to fyn: implications for tau phosphorylation in Alzheimer's disease. Acta Neuropathol Commun 4:49
53. Lauren J, Gimbel DA, Nygaard HB, Gilbert JW, Strittmatter SM (2009) Cellular prion protein mediates impairment of synaptic plasticity by amyloid-beta oligomers. Nature 457:1128–1132
54. Lewis J, Dickson DW, Lin WL, Chisholm L, Corral A, Jones G et al (2001) Enhanced neurofibrillary degeneration in transgenic mice expressing mutant tau and APP. Science 293:1487–1491
55. Lewis V, Whitehouse IJ, Baybutt H, Manson JC, Collins SJ, Hooper NM (2012) Cellular prion protein expression is not regulated by the Alzheimer's amyloid precursor protein intracellular domain. PLoS One 7:e31754
56. Li C, Gotz J (2018) Pyk2 is a novel tau tyrosine kinase that is regulated by the tyrosine kinase fyn. J Alzheimers Dis 64:205–221
57. Li R, Lindholm K, Yang LB, Yue X, Citron M, Yan R et al (2004) Amyloid beta peptide load is correlated with increased beta-secretase activity in sporadic Alzheimer's disease patients. Proc Natl Acad Sci USA 101:3632–3637
58. Masters CL, Simms G, Weinman NA, Multhaup G, McDonald BL, Beyreuther K (1985) Amyloid plaque core protein in Alzheimer disease and Down syndrome. Proc Natl Acad Sci USA 82:4245–4249
59. Mc Donald JM, Savva GM, Brayne C, Welzel AT, Forster G, Shankar GM et al (2010) The presence of sodium dodecyl sulphate-stable Abeta dimers is strongly associated with Alzheimer-type dementia. Brain 133:1328–1341
60. McMillan P, Korvatska E, Poorkaj P, Evstafjeva Z, Robinson L, Greenup L et al (2008) Tau isoform regulation is region- and cell-specific in mouse brain. J Comp Neurol 511:788–803
61. Mirra SS, Heyman A, McKeel D, Sumi SM, Crain BJ, Brownlee LM et al (1991) The Consortium to Establish a Registry for Alzheimer's Disease (CERAD). Part II. Standardization of the neuropathologic assessment of Alzheimer's disease. Neurology 41:479–486
62. Mondragon-Rodriguez S, Trillaud-Doppia E, Dudilot A, Bourgeois C, Lauzon M, Leclerc N et al (2012) Interaction of endogenous tau protein with synaptic proteins is regulated by *N*-methyl-*D*-aspartate receptor-dependent tau phosphorylation. J Biol Chem 287:32040–32053
63. Nisbet RM, Polanco JC, Ittner LM, Gotz J (2015) Tau aggregation and its interplay with amyloid-beta. Acta Neuropathol 129:207–220
64. Nygaard HB, van Dyck CH, Strittmatter SM (2014) Fyn kinase inhibition as a novel therapy for Alzheimer's disease. Alzheimers Res Ther 6:8
65. Oddo S, Billings L, Kesslak JP, Cribbs DH, LaFerla FM (2004) Abeta immunotherapy leads to clearance of early, but not late, hyperphosphorylated tau aggregates via the proteasome. Neuron 43:321–332
66. Ondrejcak T, Hu NW, Qi Y, Klyubin I, Corbett GT, Fraser G et al (2019) Soluble tau aggregates inhibit synaptic long-term depression and amyloid beta-facilitated LTD in vivo. Neurobiol Dis 127:582–590
67. Ondrejcak T, Klyubin I, Corbett GT, Fraser G, Hong W, Mably AJ et al (2018) Cellular prion protein mediates the disruption of hippocampal synaptic plasticity by soluble tau in vivo. J Neurosci 38:10595–10606
68. Ordonez-Gutierrez L, Torres JM, Gavin R, Anton M, Arroba-Espinosa AI, Espinosa JC et al (2013) Cellular prion protein modulates beta-amyloid deposition in aged APP/PS1 transgenic mice. Neurobiol Aging 34:2793–2804
69. Otvos L Jr, Feiner L, Lang E, Szendrei GI, Goedert M, Lee VM (1994) Monoclonal antibody PHF-1 recognizes tau protein phosphorylated at serine residues 396 and 404. J Neurosci Res 39:669–673
70. Parkin ET, Watt NT, Hussain I, Eckman EA, Eckman CB, Manson JC et al (2007) Cellular prion protein regulates beta-secretase cleavage of the Alzheimer's amyloid precursor protein. Proc Natl Acad Sci USA 104:11062–11067
71. Peters PJ, Mironov A Jr, Peretz D, van Donselaar E, Leclerc E, Erpel S et al (2003) Trafficking of prion proteins through a caveolae-mediated endosomal pathway. J Cell Biol 162:703–717
72. Rezaie P, Pontikis CC, Hudson L, Cairns NJ, Lantos PL (2005) Expression of cellular prion protein in the frontal and occipital lobe in Alzheimer's disease, diffuse Lewy body disease, and in normal brain: an immunohistochemical study. J Histochem Cytochem 53:929–940
73. Rijal Upadhaya A, Capetillo-Zarate E, Kosterin I, Abramowski D, Kumar S, Yamaguchi H et al (2012) Dispersible amyloid β-protein oligomers, protofibrils, and fibrils represent diffusible but not soluble aggregates: their role in neurodegeneration in amyloid precursor protein (APP) transgenic mice. Neurobiol Aging 33:2641–2660
74. Rijal Upadhaya A, Kosterin I, Kumar S, Von Arnim C, Yamaguchi H, Fändrich M et al (2014) Biochemical stages of amyloid β-peptide aggregation and accumulation in the human brain and their association with symptomatic and pathologically-preclinical Alzheimer's disease. Brain 137:887–903
75. Rijal Upadhaya A, Lungrin I, Yamaguchi H, Fändrich M, Thal DR (2012) High-molecular weight Aβ-oligomers and protofibrils are the predominant Aβ-species in the native soluble protein fraction of the AD brain. J Cell Mol Med 16:287–295
76. Roberson ED, Scearce-Levie K, Palop JJ, Yan F, Cheng IH, Wu T et al (2007) Reducing endogenous tau ameliorates amyloid beta-induced deficits in an Alzheimer's disease mouse model. Science 316:750–754
77. Salazar SV, Cox TO, Lee S, Brody AH, Chyung AS, Haas LT et al (2019) Alzheimer's disease risk factor Pyk2 mediates amyloid-beta-induced synaptic dysfunction and loss. J Neurosci 39:758–772
78. Salazar SV, Gallardo C, Kaufman AC, Herber CS, Haas LT, Robinson S et al (2017) Conditional deletion of Prnp rescues

behavioral and synaptic deficits after disease onset in transgenic Alzheimer's disease. J Neurosci 37:9207–9221
79. Schwarz AJ, Yu P, Miller BB, Shcherbinin S, Dickson J, Navitsky M et al (2016) Regional profiles of the candidate tau PET ligand 18F-AV-1451 recapitulate key features of Braak histopathological stages. Brain 139:1539–1550
80. Senthivinayagam S, McIntosh AL, Moon KC, Atshaves BP (2013) Plin2 inhibits cellular glucose uptake through interactions with SNAP23, a SNARE complex protein. PLoS One 8:e73696
81. Sepulcre J, Grothe MJ, d'Oleire Uquillas F, Ortiz-Teran L, Diez I, Yang HS et al (2018) Neurogenetic contributions to amyloid beta and tau spreading in the human cortex. Nat Med 24:1910–1918
82. Smith LM, Zhu R, Strittmatter SM (2018) Disease-modifying benefit of Fyn blockade persists after washout in mouse Alzheimer's model. Neuropharmacology 130:54–61
83. Soderberg O, Gullberg M, Jarvius M, Ridderstrale K, Leuchowius KJ, Jarvius J et al (2006) Direct observation of individual endogenous protein complexes in situ by proximity ligation. Nat Methods 3:995–1000
84. Spires-Jones TL, Attems J, Thal DR (2017) Interactions of pathological proteins in neurodegenerative diseases. Acta Neuropathol 134:187–205
85. Sturchler-Pierrat C, Abramowski D, Duke M, Wiederhold KH, Mistl C, Rothacher S et al (1997) Two amyloid precursor protein transgenic mouse models with Alzheimer disease-like pathology. Proc Natl Acad Sci USA 94:13287–13292
86. Takahashi RH, Tobiume M, Sato Y, Sata T, Gouras GK, Takahashi H (2011) Accumulation of cellular prion protein within dystrophic neurites of amyloid plaques in the Alzheimer's disease brain. Neuropathology 31:208–214
87. Thal DR, Capetillo-Zarate E, Del Tredici K, Braak H (2006) The development of amyloid beta protein deposits in the aged brain. Sci Aging Knowl Environ 2006:re1
88. Thal DR, Ghebremedhin E, Rüb U, Yamaguchi H, Del Tredici K, Braak H (2002) Two types of sporadic cerebral amyloid angiopathy. J Neuropathol Exp Neurol 61:282–293
89. Thal DR, Holzer M, Rüb U, Waldmann G, Gunzel S, Zedlick D et al (2000) Alzheimer-related tau-pathology in the perforant path target zone and in the hippocampal stratum oriens and radiatum correlates with onset and degree of dementia. Exp Neurol 163:98–110
90. Thal DR, Larionov S, Abramowski D, Wiederhold KH, Van Dooren T, Yamaguchi H et al (2007) Occurrence and co-localization of amyloid beta-protein and apolipoprotein E in perivascular drainage channels of wild-type and APP-transgenic mice. Neurobiol Aging 28:1221–1230
91. Thal DR, Rüb U, Orantes M, Braak H (2002) Phases of Abeta-deposition in the human brain and its relevance for the development of AD. Neurology 58:1791–1800
92. Thal DR, Rüb U, Schultz C, Sassin I, Ghebremedhin E, Del Tredici K et al (2000) Sequence of Abeta-protein deposition in the human medial temporal lobe. J Neuropathol Exp Neurol 59:733–748
93. Tousseyn T, Bajsarowicz K, Sanchez H, Gheyara A, Oehler A, Geschwind M et al (2015) Prion disease induces Alzheimer disease-like neuropathologic changes. J Neuropathol Exp Neurol 74:873–888
94. Um JW, Nygaard HB, Heiss JK, Kostylev MA, Stagi M, Vortmeyer A et al (2012) Alzheimer amyloid-beta oligomer bound to postsynaptic prion protein activates Fyn to impair neurons. Nat Neurosci 15:1227–1235
95. van Eersel J, Stevens CH, Przybyla M, Gladbach A, Stefanoska K, Chan CK et al (2015) Early-onset axonal pathology in a novel P301S-Tau transgenic mouse model of frontotemporal lobar degeneration. Neuropathol Appl Neurobiol 41:906–925
96. Vanmechelen E, Vanderstichele H, Davidsson P, Van Kerschaver E, Van Der Perre B, Sjogren M et al (2000) Quantification of tau phosphorylated at threonine 181 in human cerebrospinal fluid: a sandwich ELISA with a synthetic phosphopeptide for standardization. Neurosci Lett 285:49–52
97. Vasconcelos B, Stancu IC, Buist A, Bird M, Wang P, Vanoosthuyse A et al (2016) Heterotypic seeding of Tau fibrillization by pre-aggregated Abeta provides potent seeds for prion-like seeding and propagation of Tau-pathology in vivo. Acta Neuropathol 131:549–569
98. Velayos JL, Irujo A, Cuadrado-Tejedor M, Paternain B, Moleres FJ, Ferrer V (2009) The cellular prion protein and its role in Alzheimer disease. Prion 3:110–117
99. Vergara C, Houben S, Suain V, Yilmaz Z, De Decker R, Vanden Dries V et al (2019) Amyloid-beta pathology enhances pathological fibrillary tau seeding induced by Alzheimer PHF in vivo. Acta Neuropathol 137:397–412
100. Vergara C, Ordonez-Gutierrez L, Wandosell F, Ferrer I, del Rio JA, Gavin R (2015) Role of PrP(C) expression in tau protein levels and phosphorylation in Alzheimer's disease evolution. Mol Neurobiol 51:1206–1220
101. Vincent B, Sunyach C, Orzechowski HD, St George-Hyslop P, Checler F (2009) p53-Dependent transcriptional control of cellular prion by presenilins. J Neurosci 29:6752–6760
102. Voigtlander T, Kloppel S, Birner P, Jarius C, Flicker H, Verghese-Nikolakaki S et al (2001) Marked increase of neuronal prion protein immunoreactivity in Alzheimer's disease and human prion diseases. Acta Neuropathol 101:417–423
103. Wang XF, Dong CF, Zhang J, Wan YZ, Li F, Huang YX et al (2008) Human tau protein forms complex with PrP and some GSS- and fCJD-related PrP mutants possess stronger binding activities with tau in vitro. Mol Cell Biochem 310:49–55
104. Watt AD, Perez KA, Rembach A, Sherrat NA, Hung LW, Johanssen T et al (2013) Oligomers, fact or artefact? SDS-PAGE induces dimerization of beta-amyloid in human brain samples. Acta Neuropathol 125:549–564
105. Watts JC, Bourkas MEC, Arshad H (2018) The function of the cellular prion protein in health and disease. Acta Neuropathol 135:159–178
106. Whitehouse IJ, Jackson C, Turner AJ, Hooper NM (2010) Prion protein is reduced in aging and in sporadic but not in familial Alzheimer's disease. J Alzheimers Dis 22:1023–1031
107. Whitehouse IJ, Miners JS, Glennon EB, Kehoe PG, Love S, Kellett KA et al (2013) Prion protein is decreased in Alzheimer's brain and inversely correlates with BACE1 activity, amyloid-beta levels and Braak stage. PLoS One 8:e59554

Affiliations

Luis Aragão Gomes[1,2] · Silvia Andrea Hipp[3,4] · Ajeet Rijal Upadhaya[3] · Karthikeyan Balakrishnan[3,5] · Simona Ospitalieri[1,2] · Marta J. Koper[1,2,6,7] · Pablo Largo-Barrientos[7,8] · Valerie Uytterhoeven[7,8] · Julia Reichwald[9] · Sabine Rabe[9] · Rik Vandenberghe[2,10,11] · Christine A. F. von Arnim[12,13] · Thomas Tousseyn[14] · Regina Feederle[15,16,17] · Camilla Giudici[16] · Michael Willem[18] · Matthias Staufenbiel[9] · Dietmar Rudolf Thal[1,2,3,14]

1 Laboratory for Neuropathology, Department of Imaging and Pathology, KU-Leuven, Leuven, Belgium

2 Leuven Brain Institute, KU-Leuven, Leuven, Belgium

3 Laboratory for Neuropathology, Institute of Pathology, University of Ulm, Ulm, Germany

4 Anasthesiology and Intensive Medicine, University Hospital of Tübingen, Tübingen, Germany

5 Department of Gene Therapy, University of Ulm, Ulm, Germany

6 Laboratory for the Research of Neurodegenerative Diseases, Department of Neurosciences, KU Leuven (University of Leuven), Leuven, Belgium

7 VIB, Center for Brain and Disease Research, Leuven, Belgium

8 Department of Neurosciences, KU-Leuven, Leuven, Belgium

9 Novartis Institutes for Biomedical Sciences, Basel, Switzerland

10 Experimental Neurology Group, Department of Neurosciences, KU Leuven, Leuven, Belgium

11 Department of Neurology, UZ-Leuven, Leuven, Belgium

12 Department of Neurology, University of Ulm, Ulm, Germany

13 Clinic for Neurogeriatrics and Neurological Rehabilitation, University- und Rehabilitation Hospital Ulm (RKU), Ulm, Germany

14 Department of Pathology, UZ Leuven, Leuven, Belgium

15 Institute for Diabetes and Obesity, Monoclonal Antibody Research Group, Helmholtz Zentrum München, German Research Center for Environmental Health (GmbH), Munich, Germany

16 German Center for Neurodegenerative Diseases (DZNE) Munich, 81377 Munich, Germany

17 Munich Cluster for Systems Neurology (SyNergy), 81377 Munich, Germany

18 Chair of Metabolic Biochemistry, Biomedical Center (BMC), Faculty of Medicine, Ludwig-Maximilians-University Munich, 81377 Munich, Germany